

1 **Ocean surface and bottom water conditions, iceberg drift and sediment transport on**  
2 **the North Iceland margin during MIS 3 and MIS 2**

3

4

5

6 Andrews, J.T.<sup>1</sup>, Smik, L.<sup>2</sup>, Belt, S.T.<sup>2</sup>, Sicre, M-A<sup>3</sup>, McCave, I. N.<sup>4</sup>

7

8 1. Institute of Arctic and Alpine Research, and Department of Geological Sciences,  
9 University of Colorado, Boulder, CO 80303

10 2. Biogeochemistry Research Centre, School of Geography, Earth and  
11 Environmental Sciences, University of Plymouth, Drake Circus, Plymouth, PL4  
12 8AA, UK.

13 3. LOCEAN, CNRS, Sorbonne Université, Campus Pierre et Marie Curie, 4 place  
14 Jussieu, Paris, France.

15 4. Godwin Laboratory for Palaeoclimate Research, Department of Earth Sciences,  
16 University of Cambridge, Downing Street, Cambridge CB2 3EQ, U.K.

17

18 **Orcid:** Andrews: 0000-0003-3169-5979

19 **Orcid:** Belt: 0000-0002-1570-2924

20 **Orcid:** Sicre: 0000-0002-5015-1400

21 **Orcid;** McCave: 0000-0002-4702-5489

22

23

24 andrewsj@colorado.edu

25

26 **Key words:** Iceland Plateau, MIS 2 and 3, sea ice biomarkers, IP<sub>25</sub>, alkenones,

27 sortable silt, sediment provenance

28

29

30 **Abstract**

31 Radiocarbon dates and marine tephra suggest that the upper 10 m of core MD99-2274,  
32 off North Iceland, extends from ~0 to ~65 ka BP. A multi-proxy sediment and biomarker  
33 study at a millennial-scale resolution is used to derive a paleoclimate scenario for this  
34 area of the southwestern Nordic Seas, which during the Holocene had intermittent  
35 excursions of icebergs and a seasonal cover of drifting sea ice across the site. The  
36 sortable silt mean size ( $\overline{SS}$ ) suggests a bottom current (1000 m depth) flow speed  
37 maximum to minimum range of ~8 cm/s during Marine Isotope Stages 2 to 3, but the data  
38 are unreliable for the Holocene. Slow-down in flow speeds may be associated with  
39 massive ice and water discharges linked to the Hudson Strait ice stream (H-events) and to  
40 melt of icebergs from Greenland in the Nordic seas where convection would have been  
41 suppressed. Five pulses of sediment with a distinct felsic component are associated with  
42 iceberg transport from E/NE Greenland. Sea ice, open water and sea surface temperature  
43 (SST) biomarker proxies (i.e. IP<sub>25</sub>, HBI III, brassicasterol and alkenones) all point  
44 towards near-perennial sea ice cover during MIS 3 and 2, rather than seasonal sea ice or  
45 open water conditions. Indeed, our biomarker and sediment data require that the seas  
46 north of Iceland experienced a nearly continuous cover of sea ice, together with icebergs  
47 calved from ice stream termini, which drifted southward. The cross-correlation of the  
48 quartz % records between MD99-2274 and the well-dated core PS2644 in Blosseville  
49 Basin indicates significant coherence in the records at a multi-millennial (~8 ky)  
50 timescale. A transition to open ocean conditions is evident from the early Holocene  
51 onwards, albeit with the occurrence of some drift ice and icebergs.

52

53

54

## 55 **1. Introduction**

56

### 57 *1.1 Aims of study*

58 In order to gain some understanding of the complex marine environments that prevailed  
59 during the Late Quaternary we need to employ a multi-proxy approach that not only  
60 characterizes ocean surface and bottom water conditions, but also provides direct  
61 measurement of glacial influences on sediment supply. Several studies have been  
62 reported from the North Iceland Shelf (Fig. 1) that document late glacial/Holocene  
63 records (e.g. Andrews et al., 2018; McCave and Andrews, 2019a & b; Sicre et al., 2008;  
64 Knudsen et al., 2003) but there are only limited references to conditions during Marine  
65 Isotope Stages (MIS) 2, 3 or 4. Therefore, with the primary goal of establishing a  
66 framework for environmental conditions in this sector of the Iceland Sea from MIS 2 to  
67 MIS 4, we selected a previously unstudied core, MD99-2274 (Labeyrie et al., 2003) (Fig.  
68 1), and sampled the upper 10 m. MD99-2274 (henceforth #2274) is a 10-cm diameter 26  
69 m Calypso core retrieved from 67.582°N and 17.073°W at 1000 m water depth (Labeyrie  
70 et al., 2003) during the IMAGES V cruise aboard the French RV *Marion Dufresne*. For  
71 further context, we note that the core site is located 200 km east of the well-studied core  
72 PS2644 (van Kreveld et al., 2000; Voelker, 1999; Voelker and Haflidason, 2015) and 163  
73 km from core P57-7 (Sejrup et al., 1989) (Table 1, Fig. 1A). The main questions we  
74 posed were: 1) what is an appropriate depth/age model, 2) is there evidence for either  
75 pervasive sea ice or an ice shelf (Boers et al., 2018; Dokken et al., 2013; Petersen et al.,  
76 2013), which have been called for to explain D-O cycles, 3) what were sea surface  
77 temperatures (SSTs), and 4) are there substantial changes in grain-size and mineral  
78 composition that can be associated with changes in bottom current flow speed and

79 changes in glacial sediment provenance? Given the location of the core (Fig. 1A) we  
80 were particularly interested in whether we could discriminate between glacial sediments  
81 derived from Iceland versus those from E/NE Greenland.

## 82 *1.2 Present-day oceanography*

83 The Iceland and Greenland Seas (Fig. 1A) are key areas for the formation of dense  
84 overflow waters (Brakstad et al., 2019) that flow south through sills in the  
85 ScotlandGreenland Ridge (Fig. 1C). The North Icelandic Jet (NIJ) flows southwestward  
86 along the slope below ~1000 m (Fig. 1C) with a mean speed of  $9.3 \text{ m} \pm 2.7 \text{ m/sec}$  towards  
87 Denmark Strait (Mauritzen, 1996; Pickart et al., 2005) where it exits to form a major  
88 component of North Atlantic Deep Water “....and points to the Iceland Sea as an  
89 *important place for this water mass formation.*” (Jonsson and Valdimarsson, 2004). The  
90 study site lies in a sensitive area with the surface flow being the East Icelandic Current  
91 (EIC), which brings cold and relatively fresh surface water as a spin-off from the East  
92 Greenland Current (EGC), whereas the North Icelandic Irminger Current (NIIC), sourced  
93 from the southern warmer and saltier waters of the North Atlantic Drift (Stefansson,  
94 1962), continues as an eastward flow over the inner North Iceland Shelf (NIC) (Fig. 1C).

95 Sea ice in the form of drift ice has been noted to reach the area in modern times,  
96 although the average position of the sea ice edge (30% sea ice cover by area) lies north of  
97 our site (Divine and Dick, 2006) (Fig. 1C). Thirty years of observations on the presence  
98 of icebergs (Andrews et al., 2019), their Fig. 7A) indicate that icebergs from E/NE  
99 Greenland drift across the site.

101 *1.3 Background to study region*

102 Stein and colleagues (Nam et al., 1995; Stein, 2008; Stein et al., 1996) studied a  
103 comprehensive suite of cores on the Scoresby Sund Trough Mouth Fan (Fig. 1A, TMF)  
104 and reported both ice-rafted debris (IRD) and  $d^{18}O$  on the near-surface planktonic  
105 foraminifera *Neoglobquadrina pachyderma* (Table 1). The cores included discrete IRD  
106 peaks (counts  $10\text{ cm}^3 > 500\ \mu\text{m}$ ), which they suggested may have been coeval with the  
107 massive ice and water discharges of the Hudson Strait Heinrich (HS H-) events (Andrews  
108 and Voelker, 2018b; Heinrich, 1988; Hemming, 2004; Hesse 2016). However, whether  
109 the response of the Greenland, Iceland, and European ice sheets was synchronous or  
110 asynchronous with the Laurentide Ice Sheet collapse events still requires clarification  
111 (Dowdeswell et al., 1999; Elliot et al., 2001). Verplanck et al (2009) provided radiogenic  
112 isotope data fingerprinting sediment sources from two cores on the Scoresby Sund TMF  
113 (O'Cofaigh et al., 2002) (JR51-GC31 and -GC32) and another core (PS62/017-4) from  
114 the Blosseville Basin (Milo et al., 2005) (Table 1). Stein et al. (1996) and Verplanck et al.  
115 (2009) described events in cores PS1730 and PS62/017-4 (Table 1, Fig. 1) that they  
116 considered coeval with the HS H-events. Andrews and Voelker (2018) have argued that  
117 the use of the term “Heinrich events” for locations such as the Nordic Seas is not  
118 appropriate and should be modified. For example, the IRD-rich layer in PS2644  
119 correlated with HS H-2 (Voelker et al., 1998) is now referred to as PS2644 IRD#2  
120 (Andrews and Voelker, 2018). In our study, events that might correlate with HS H-events  
121 will be termed #2274-IRD#.

122       There is no firm agreement on the extent and duration of sea ice cover in the

123 Nordic Seas during MIS 2 and MIS 3. The CLIMAP data showed an extensive cover  
124 across the Nordic Seas (Ruddiman and McIntyre, 1981) whereas Sarnthein et al. (2003)  
125 argue that the Nordic Seas during MIS 2 were “..largely ice free” during the summer  
126 months. The presence of an ice shelf buttressing the East Greenland ice streams has also  
127 triggered a debate especially as to a possible answer to the cause of D-O oscillations  
128 (Pettersen et al., 2013; van Kreveld et al., 2000). However, other researchers working at  
129 sites in the eastern Nordic Seas have rather focused on the role of sea ice (Dokken et al.,  
130 2013; Hoff et al., 2016) and changes in the structure of the water column, and concluded  
131 that during Greenland interstadials in MIS 3, sea ice was limited in extent and duration.

132       The presence of thick, pervasive sea ice could potentially limit the export of  
133 icebergs from E and NE Greenland Ice Streams (Reeh et al., 1999), although the sediment  
134 records from numerous sediment cores retrieved from the floor of the Arctic  
135 Ocean clearly document that iceberg rafting occurred throughout the Pleistocene (Clark,  
136 1990a,b; Stein, 2008; Phillips and Grantz, 2001; Stokes et al., 2005), with some evidence  
137 that the timing of events in some cores were similar to those for HS H-events. For  
138 example, IRD peaks in cores from the Arctic Ocean were linked to the McClure Ice  
139 Stream in the NW sector of the Laurentide Ice Sheet and dated at 12.9, 15.6, ~22, and 30  
140 ka BP (Stokes et al., 2005). Iceberg drift is primarily a function of the integrated current  
141 direction and speed over depth, plus a component associated with wind forcing on the  
142 exposed “sail” (Bigg, 2016). In many ways, sea ice protects icebergs as it inhibits wave  
143 action, which is the greatest cause of iceberg disintegration (Bigg, 2016; Venkatesh et al.,  
144 1994).

145 *1.4 Ice sheet extent MIS 1 to MIS 3*

146 #2274 lies only 60 km north of the LGM limit of the Iceland Ice Sheet (IIS) (Fig. 1)  
147 (Andrews and Helgadottir, 2003; Patton et al., 2017) with the onset of retreat associated  
148 with calibrated radiocarbon dates of between 14 and 15 ka BP, depending on the ocean  
149 reservoir correction (Andrews et al., 2018; Andrews and Helgadottir, 2003; Knudsen et  
150 al., 2003). Retreat from the maximum position was rapid (Andrews et al., 2018; Norðdahl  
151 and Ingolfsson, 2015; Patton et al., 2017), and the ice sheet was at or behind the  
152 presentday coast by the time of the deposition of the Vedde tephra ~12.2 ka BP (Lohne et  
153 al., 2013). Little detail is known about the history of this ice sheet during MIS 3 (e.g.  
154 Andrews et al., 2017). Moles et al. (2019) argued that the North Atlantic Ash Zone II  
155 (NAAZII) tephra, dated ca 54 ka BP (Austin and Hibbert, 2012), was erupted under >400  
156 m of ice, thus indicating a reasonably extensive IIS during the Greenland <sup>18</sup>O stadial 15.2  
157 (Moles et al., 2019; Rasmussen et al., 2014), but no specific information is currently  
158 available on the MIS 3 history of the ice sheet.

159       The Greenland Ice Sheet (GIS) extended to the shelf break during the LGM  
160 (Funder et al., 2011b; Vasskog et al., 2015) but little is known about its history during  
161 MIS 3 or MIS 4. Judging from the delivery of quartz-rich sediments to cores along  
162 Denmark Strait, especially PS2644 and MD99-2323 (Andrews and Vogt, 2020a), it is  
163 probable that the ice also reached a similar position at these times. Peterson et al. (2013)  
164 suggested that an ice shelf may have extended out from the East Greenland Shelf across  
165 Blosseville Basin, although the sedimentary evidence for this is scanty (Andrews and  
166 Vogt, 2020a).

167



168 *1.5 Bedrock Geology and source signatures*

169 In terms of the mineral composition of #2274 sediments, the bedrock in glacial source  
170 areas consists primarily of either mafic (basalt) or felsic (granites/gneisses/sandstones),  
171 although finer source identification is possible (Andrews and Vogt, 2014; 2020) (Fig.  
172 1A). Further, Andrews and Vogt (2014) demonstrated that the sediment mineral  
173 signature of sediments offshore from the Caledonian Fold Belt was dominated by high  
174 wt% of quartz, illite, and muscovite. Detrital carbonate sediments derived from the  
175 Paleozoic outcrops of N Greenland and the Canadian Arctic are also recognized by color  
176 and mineralogy. However, radiogenic isotopes (White et al., 2016; Verplanck et al.,  
177 2009) allow more age-related differentiations, which in terms of our region (Fig. 1A and  
178 B), consists of Archaean, Paleoproterozoic, Caledonian Fold Belt, and Tertiary volcanics  
179 (Henriksen, 2008).

180 **2. Environmental proxies and age model**

181 *2.1 Data methods*

182  
183 The proxies used in this paper are the sea ice biomarkers IP<sub>25</sub> and HBI II (Belt et al.,  
184 2007; Belt and Müller, 2013; Belt, 2018), brassicasterol and HBI III as indicators of open  
185 water primary production (Volkman, 1986; Belt et al., 2015), alkenones (for SST) (Sicre  
186 et al., 2008a), % C37:4 alkenone to identify polar surface waters, grain-size indicators of  
187 bottom flow and deposition (McCave and Andrews, 2019a, b; McCave et al., 2017),  
188 magnetic susceptibility, and quantitative X-ray diffraction estimates of mineral wt%  
189 (Andrews et al., 2017; Andrews and Vogt, 2014). The X-ray diffraction data for #2274  
190 are available (Andrews and Vogt, 2020b) The full details of these methods are included  
191 as Supplementary Material.

192

## 193 2.2 Depth/age model

194 The age model is based on radiocarbon dates and the occurrence of tephras (Table 2).

195 There are significant problems associated with obtaining and interpreting calibrated ages

196 because of the uncertainty of the ocean reservoir correction (ORC), which has varied

197 spatially and temporally, and might be as much as 1000 yr (Andrews et al., 2018; Skinner

198 et al., 2019; Voelker, 1999; Voelker et al., 1998). Three radiocarbon dates were obtained

199 on the near-surface planktonic foraminifera *Neogloboquadrina pachyderma* and the other

200 on lustrous shell fragments. Most tephras older than the Borrobol (ca 14.5 ka BP) (Lind et

201 al., 2016; Matthews et al., 2011) are dated by reference to GIS cores, which themselves

202 are based on a variety of assumptions and whose error increases with the estimated age

203 (Boers et al., 2017). The qXRD data (Andrews et al., 2013; 2018) suggest the presence of

204 high wt% of volcanic glass in two cores on the Iceland Shelf that might be coeval with

205 the Vedde and NAAZII tephras (Brendryen et al., 2011; Lohne et al., 2013). The tephra

206 bed at 607 cm in #2274 was identified by Haflidasson (person. commun. 2018) as being

207 similar to FMAZ IV dated at ~47.12 ka BP (Davies et al., 2008; Rasmussen et al., 2003;

208 Voelker and Haflidason, 2015) and that date is used in our depth/age models (see

209 Supplementary Material). Other discrete layers of black basaltic glass were noted in the

210 shipboard log at 99, 127.5, 717, and 740 cm (Labeyrie et al., 2003, p 477), and age

211 estimates were obtained from our depth/age model (see later).

212 We used the Bayesian radiocarbon calibration program “Bacon” (Blaauw and

213 Christen, 2005) to construct depth/age models, but we also acknowledge the many

214 problems associated with establishing accurate depth/age models (Telford et al., 2003;

215 Trachsel and Telford, 2017). The first model is based solely on the available <sup>14</sup>C dates and

216 the 607 cm tephra (Table 2A and B), while the second one is based on an assumed age  
217 estimate for the core top of  $500 \pm 500$  (i.e. little sediment loss) and the inferred presence  
218 of the Vedde and NAAZII tephras. Given the uncertainty in the OCR, we used a  $DR = 0$ .  
219 In practice, there is relatively little difference in the median age estimates (Fig. 2A). The  
220 average sediment accumulation rate (SAR) is 68 yr/cm or 14.7 cm/ky, thus our 10 cm  
221 sampling density permits millennial-scale evaluations, with an average spacing between  
222 samples of 0.5 cal ky. Remarkably, for MD cores of this vintage (1999), the upper part of  
223 the core shows no evidence of piston-induced stretching (Skinner and McCave, 2003).  
224 However, the spread between minimum and maximum age estimates is often  
225 considerable given the relative paucity of dated levels, and the Bayesian approach results  
226 in an age estimate for the core top of 3600 yr BP, although the estimated date of  $500 \pm$   
227  $500$  yr BP finds some support in our data. The estimated ages for the logged tephra layers  
228 are: ~11, 13.2, 53, and 56 ka BP. A possible age for the 99 cm basaltic tephra is the  
229 10.2 ka BP Saksunarvatn tephra (Lohne et al., 2013), which is widespread on the north  
230 Iceland Shelf (Krisjansdottir et al., 2007; Eiriksson and Knudson, 2002). All our  
231 subsequent data have been converted to a common depth/age model using the data in  
232 Table 2B; thus, robust inter-proxy comparisons can be made. To ensure that we have not  
233 forced our data into an existing framework we have not tuned our model to other records  
234 (Blaauw, 2012).

235 We have also obtained radiocarbon dates on several *Vema* cores that were taken  
236 to the north of Iceland and #2274 (Fig. 1; Table 3) (Manley and Jennings, 1996). The  
237 calibrated radiocarbon dates range from ~13 to > 49 ka BP ( $DR = 0$ ) and were obtained  
238 on relatively large samples of *N. pachyderma* (Table 3). Several tephras were noted in the

239 core description (Suppl. Data), thus indicating that conditions allowed for the deposition  
240 of discrete tephras. The dates from these cores also provide additional information on the  
241 presence of significant numbers of the planktonic foraminifera *N. pachyderma* (Greco et  
242 al., 2019) and hence inferences about sea ice cover and light conditions.

### 243 **3. Results**

244

#### 245 *3.1 Lithology and Grain-size*

246 The core log of core #2274 (Labeyrie et al., 2003. p. 477) described the sediment as  
247 being principally mottled silty clay with colors ranging between 2.5Y4/2 to 5Y4/1.  
248 Visible ice-rafted clasts occur but are not common. The grain-size measurements were  
249 undertaken on sample splits from the qXRD samples and only 30 samples were  
250 processed, resulting in a coarse resolution data set (on average one sample every 2300  
251 yr). The sediments vary between a very coarse to a fine silt with average grain-sizes  
252 varying between 54.3 to 6.05  $\mu\text{m}$ . Sand > 240  $\mu\text{m}$  is considered to be ice-rafted (McCave  
253 and Andrews, 2019a) and occurs in low % throughout the core, except for two notably  
254 coarser intervals with IRD<sub>240</sub> > 5%, (Fig. 3).

255 We have also undertaken an analysis of the sortable silt mean size ( $\bar{SS}$ ) and SS%  
256 in the 63-10  $\mu\text{m}$  fractions (McCave et al., 1995). The correlation coefficient between  
257 these two variables is  $r = 0.804$  indicating, relative to other cores (McCave and Andrews,  
258 2019a,b), a somewhat noisy correlation, but a generally current-sorted signal  
259 (Supplementary Fig. 1). Computation of the running correlation between SS% and  $\bar{SS}$   
260 yields high average values ( $r > 0.9$ ) between ~11 and 42 ka BP but values unacceptable  
261 for flow speed inference occur in the Holocene and during brief interval ~57 ka BP ( Fig.  
262 3). Variations in the flow speed of bottom currents (Fig. 1C) in this region reflect

263 changes in the vigour of the ocean overturning system because the NIJ feeds into the  
264 Denmark Strait overflow, a key starting point for the North Atlantic western Boundary  
265 Undercurrent.

266 The overall range (minimum-maximum) in flow speed indicated by this record is  
267 ~8 cm/s. Calibration of the sortable silt proxy yields a sensitivity ( $\text{cm s}^{-1}/\mu\text{m}$ ) rather than  
268 an absolute speed-size relationship (McCave et al., 2017). In favourable circumstances  
269 actual speeds may be estimated by matching core-top  $\overline{\text{SS}}$  data to nearby current meter  
270 measurements and plotting the differences downcore. Unfortunately, because the  
271 Holocene data are unreliable as a speed record, we cannot relate this to the present nearby  
272 flow speed measurements of 9.3 cm/sec (Jonsson, 2004). Nevertheless, low speeds  
273 correspond to HS H 1 (~15 ka), 4 (~40 ka), and 6 (~60 ka) (Fig. 3) as expected from  
274 previous work on the impact of Heinrich and other cold events on N. Atlantic circulation  
275 (e.g. Kleiven et al., 2011), on the basis of which, speeds of <5 cm/s are probable.

276

### 277 *3.2 Mineral composition*

278 On Figure 4, we plot the changes in the weight % of key minerals as determined by  
279 qXRD as well as the ratio quartz/pyroxene, which we use as a measure of felsic/mafic  
280 bedrock (as opposed to quartz/plagioclase which was used by Moros et al. (2004)). The  
281 quartz wt% in a surface grab from this site is ~5% (Andrews and Eberl, 2007), and the  
282 median for the whole record is 5.3 % with a maximum of 16.8 %. The magnetic  
283 susceptibility record for #2274 (Fig. 2A) is clearly inversely associated with the  
284 variations in quartz (Fig. 2B), which, together with the K-feldspars, are diamagnetic  
285 minerals (Robinson et al., 1995; Watkins and Maher, 2003). A similar inverse

286 relationship was noted in other cores from the area (Andrews and Vogt, 2020a). Hence  
287 the magnetic susceptibility fluctuations support our interpretation that there are  
288 substantial variations in the inputs of felsic- versus mafic-rich sediments.

289         The Holocene record mimics that from many sites on the North Icelandic Shelf  
290 (NIS) in showing an increase in quartz toward the present-day (Andrews et al., 2019).  
291 Quartz and pyroxene have an antiphase relationship ( $r^2 = 0.47$ ), which in part is related to  
292 the mineral data summing to 100% (i.e. a closed array), and which provides some  
293 constraints on the interpretation (Aitchison, 1986; Chayes, 1971). There are five  
294 sustained peaks in the quartz wt % (Fig. 4), and K-feldspar (not shown, K-feldspar values  
295 track those of quartz (Andrews and Vogt, 2020a)) are therefore not included in this  
296 figure), which we interpret as indicating the influx of sediment from NE Greenland and  
297 possibly farther afield from Canada or Fennoscandia. Of these possible mechanisms,  
298 icebergs alone carry basal and englacial debris that includes all size fractions from  
299 cobbles to clay ( $> 1 \mu\text{m}$ ). The variations in quartz are frequently matched by the sum of  
300 calcite and dolomite (carbonate) (Fig. 4) ( $r^2 = 0.13$ ,  $p < 0.0001$ ) although the correlations  
301 are much more significant for dolomite ( $r^2 = 0.22$ ) than calcite ( $r^2 = 0.07$ ). This probably  
302 represents transport of glacially derived material from the carbonate bedrock of NE and  
303 N Greenland and/or the Canadian Arctic Islands and Channels (Darby and Zimmerman,  
304 2008; Lakeman et al., 2018; Phillips and Grantz, 2001). The estimated ages for the 5  
305 peaks are 14.4, 31.5, 40, 54.7, and 61.8 ka BP (Fig. 4) with a possible smaller episode  
306 ~22.8 ka BP. These age estimates are somewhat similar to the HS H-events (Andrews  
307 and Voelker, 2018a; Heinrich, 1988; Hemming, 2004) (see Fig. 3) but their duration are

308 longer than the <1 ky episodes of detrital carbonate deposition associated with the HS  
309 Hevents (Andrews and Voelker, 2018a).

310 Previous work on sediment sources in this area (Verplanck et al., 2009) provide  
311 temporally limited but critical information using radiogenic isotopes on the < or > 63 $\mu$ m  
312 fractions. Debris flow from the two Scoresby Sund TMF sites (JR51-GC31,-32, Table 1,  
313 Fig. 1B) lay along the 1.7 Ga Paleoproterozoic isochron; the samples contained abundant  
314 quartz and lesser amounts of basalt (Verplanck et al., 2009, p.53). However, the  
315 sediments in the Blossville Basin (core 17-4, Fig. 1A, Table 1), some 150 km  
316 downstream (Fig. 1A), and considered to be coeval with HS H events-1, -2, and -3, all  
317 cluster along the 0.5 Ga isochron (Caledonide bedrock, that outcrops on the eastern edge  
318 of NE Greenland north of Scoresby Sund (Fig. 1B)). The same isotopic signature  
319 characterized the non-HS H sediments in this core. Pb systematics indicate that the  
320 Holocene sediment samples at sites 907 (Table 1) and JR51-GC28 are dominated by the  
321 0.5 Ga Caledonides (White et al., 2016). Given the sediment SedUnMix results (Fig. 5)  
322 and the reported radiogenic isotopic data (Verplanck et. al., 2009; White et al., 2016), the  
323 variations in quartz are most probably associated with sediment discharge events from  
324 glacial erosion and transport in ice streams flowing through the numerous fiords north of  
325 Scoresby Sund and primarily within the Caledonian Fold Belt outcrop (Evans et al., 2002,  
326 2009; Stein, 2008).

327 The SedUnMix analysis included sediments from NE Greenland (Caledonides,  
328 ~73N; Andrews et al., 2016), E Greenland (basalt), and Iceland. The analysis of possible  
329 bedrock sources for the #2274 compositional changes indicated (as might be expected  
330 given the bedrock geology of E and NE Greenland, and Iceland) that the NE Greenland

331 source had a granite and gneissic composition, whereas E Greenland and Iceland were  
332 linked to basalt and also dolerite (Brooks and Nielsen, 1982; Henriksen, 2008; Higgins et  
333 al., 2008; Kristjansson et al., 1979). The results (Fig. 5) indicate that felsic-rich sediments  
334 from NE Greenland or farther afield (Arctic Canada, Fennoscandia) (Verplanck et al.,  
335 2009) were deposited in a series of events that mimic the influx of quartz to the site (Figs.  
336 2B and 4); the correlation between the NE Greenland Calendonides source estimates in  
337 #2274 and the quartz wt% explains 79% of the variance. The average “unaccounted” or  
338 “unexplained” composition averaged  $20 \pm 5$  % and degree of fit or average absolute bias  
339 is  $2.3 \pm 0.4$  wt% indicating that the input mineral source regions provide a good fit to the  
340 #2274 mineral compositions. Figure 5 highlights two periods when the mineral  
341 composition indicates little deposition of sediment that could be ascribed to a felsic  
342 source centered around 20 and 57 ka BP, the latter being a time of substantial deposition  
343 of tephra at this site and also a time when glacial ice covered at least some of Iceland  
344 (Moles et al., 2019). Source estimates from E. Greenland (sites seaward of the early  
345 Tertiary basalt outcrop on the Geikie Plateau) and SW Iceland resulted in nearly identical  
346 patterns over the last ~65 ka BP (Fig. 5), but the results from considering Icelandic basal  
347 glacial marine diamictons (Dmm) as a source are different. The reasons for these two  
348 differing estimates are presently unclear.

349 The provenance time-series thus suggests that we can identify four episodes in the  
350 arrival of foreign sourced sediments; 1) from ~65 to 38 ka BP when distinct pulses of NE  
351 Greenland sourced sediments arrived; 2) 38 to 17 ka BP when there was an overall  
352 decrease in this source with virtually no quartz noted ~20 ka BP; 3) a large pulse of these  
353 sediments centered ~ 15 ka BP; and 4) the last 10 ka or so that shows a steady increase in



354 this source. This latter event is also noted in MD99-2269 (Fig. 7) and is matched by  
355 changes in the sea ice biomarker IP<sub>25</sub> (Cabedo-Sanz et al., 2016).

### 356 *3.3 Biomarkers*

357 The sea ice biomarkers IP<sub>25</sub> and HBI II were absent or below the limit of detection in the  
358 majority of the sediment sections analyzed with only a few exceptions (Fig. 6). Of the  
359 two, HBI II was always more abundant, consistent with findings from previous studies  
360 from the study region and elsewhere in the Arctic (e.g. Massé et al., 2011; Xiao et al.,  
361 2013; Bai et al., 2019). In some cases, only HBI II could be identified and quantified,  
362 with IP<sub>25</sub> likely also present in such horizons but below the detection limit.

363 Alkenones and brassicasterol were found at very low concentrations in glacial  
364 sediments contrasting with higher abundances in Holocene sediments. Further, the open  
365 water biomarker HBI III was only detected in Holocene sediments (data not shown).  
366 While alkenone-SSTs ranged from 7 to 9°C during the Holocene, they are unexpectedly  
367 high in the glacial portion of the record, spanning from 8 to 16°C.

368

## 369 **4. Discussion**

### 370 *4.1 Icebergs and IRD during MIS 3 and MIS 2*

371 There is no general theory about the association of sea ice and icebergs and there is no  
372 observational census of the icebergs being transported in the EGC as there is for the  
373 Labrador Shelf off Newfoundland, apart from a 30-yr count of icebergs on the Iceland  
374 shelves (Jónsdóttir *in* Andrews et al., 2019). However, Cabedo-Sanz et al. (2016) and  
375 Darby et al. (2017) showed that Holocene variations in the wt% of quartz and the sea ice  
376 biomarker IP<sub>25</sub> co-varied in cores to the west and south of #2274, yet this was not the case

377 at #2274 during MIS 2 and MIS 3 (Figs. 4 and 6). In N Greenland, semi-permanent  
378 seaice conditions prevail today and did so intermittently during the Holocene (Funder et  
379 al.,  
380 2011a) and it is reasonable to assume that sea-ice would have been more extensive during  
381 MIS 2 and MIS 3 when the GIS may have reached the shelf break. However,  
382 cosmogenic dates pertaining to the extent of the Northeast Greenland Ice Stream at  
383 ~78°N (Larsen et al., 2018) have been used to argue that this ice stream was behind its  
384 present margin “...41-26 ka.”

385         Several authors have argued for the presence of an ice shelf fringing the E/NE  
386 GIS (Boers et al., 2018; Petersen et al., 2013). However, sediments recovered from  
387 beneath ice shelves are invariably fine-grained and lack ice-rafted debris (Domack et al.,  
388 1999; Jennings et al., 2019; McKay et al., 2016), whereas the sediments from the  
389 Scoresby Sund TMF (Fig. 1) and margin contain clear IRD (Stein et al., 1996) (Fig. 5; see  
390 also Table 3). Radiocarbon dates in Stein et al., (1996a) were based on 2000 *N.*  
391 *pachyderma* specimens per sample, and the numerous MIS 2 and MIS 3 radiocarbon  
392 dates on *N. pachyderma* from PS2644 (Sarnthein et al., 2003; Voelker, 1999; Voelker et  
393 al., 1998, 2000) were obtained on 10 mg samples of 800-2300 tests in 1-cm sediment  
394 samples. Although the complete ecology of *N. pachyderma* is not well known, a study of  
395 plankton hauls (Greco et al., 2019) indicates a relationship between sea ice cover and  
396 chlorophyll, hence suggesting that “*light or light-dependent processes might influence*  
397 *the ecology of this species.*” In addition, several of these cores have discrete tephra layers  
398 indicating rapid accumulation of tephras by particles falling through the water column,  
399 versus a more dispersed occurrence if the tephra was deposited on multi-year sea ice.

400 Together these data indicate that the sea ice, at times during MIS2 and 3 and probably  
401 seasonally, must have had extensive leads and open-water areas(see also Fig. 4 in  
402 Sadatzki et al., 2020).

403 Stein et al (1996) present detailed IRD data (counts  $10 \text{ cm}^3 > 500 \mu\text{m}$ ) from a  
404 series of radiocarbon dated cores on the Scoresby Sund TMF (Fig. 1; PS1726 and  
405 PS1730, Fig. 1B) that reflect delivery of coarse sediments in a discrete series of episodes  
406 (data from [www.Pangaea.de](http://www.Pangaea.de)). Stein (2008) noted coarse sediment intervals that were  
407 attributed to iceberg-rafting at ~4-15, 16, 17-18, 20-21, and 22-23 ka BP. There are no  
408 mineral composition data for PS1730, but data exist for PS2644, which is 300 km away  
409 (Table 1, Fig. 1B) (Andrews and Vogt, 2020a; Vogt, 2017). A comparison between  
410 PS2644 and #2274 (Fig. 8A) indicates that PS2644, closer to the Scoresby Sund Ice  
411 Stream, has more quartz wt% but there are some notable corresponding peaks in both  
412 series. However, we note that the quartz wt% were obtained via two different but  
413 comparable quantitative methods (Andrews and Vogt, 2020a; Vogt, 2017; Zou, 2016). To  
414 evaluate similarities and differences between these two sites we used cross-wavelet  
415 analysis (Roesch and Schmidbauer, 2018; Hammer et al., 2001) (Fig. 8). The wavelet  
416 analysis of the two quartz records (Fig. 8A) demonstrates both important coeval events as  
417 well as obvious differences. In addition, the overall match between these sites for the  
418 earlier part of the record adds confidence to our age model, and also emphasizes the  
419 important differences between 35 and 65 ka. The reconstructed wavelets for PS2644  
420 show three major pulses of quartz at ~13, 20, and 29 ka BP, and these are matched by  
421 much lower peaks at #2274. Conversely, there are no distinct peaks during MIS 3 in  
422 PS2644 but there are in #2274. The sense of the directional arrows in Figure 8B is that

423 PS2644 either leads or is in phase with #2274, and there is a hint of a significant shorter  
424 period ~60 ka BP with the two records being anti-phase. The cross-wavelet power  
425 spectrum (Fig. 8B) confirms the presence of a significant zone of coherence extending  
426 from ~10-34 ka BP with the average cross-wavelet power peaking at ~8 ky (Fig. 8C); this  
427 is of course similar to the periodicity of HS H-events (see Clark et al., 2007) (e.g. Fig. 3)  
428 but lacks the diagnostic carbonate provenance indicators (Andrews and Voelker, 2018).  
429 Possibly because of our 0.6 ky sample spacing (Fig. 8A), there is no obvious D-O signal  
430 in the quartz PS2644 data, whereas it is evident in the  $\delta^{18}\text{O}_{Np}$  data (Suppl. Fig. 3). The  
431 difference in signals between #2274 and PS2644 during MIS 3 (Fig. 8A) suggests a  
432 change in either the delivery of quartz-rich sediments or a dampening down of sediment  
433 delivery.

434         The sortable silt evidence indicates that even at the glacial maximum there was  
435 flow along the slope in the precursor to the NIJ. As this presently heads toward the  
436 Denmark Strait outflow, we suggest that the Nordic Seas acted as a source of deep waters  
437 (probably formed in the east where Atlantic inflow continued (Sarnthein et al, 1994)) that  
438 overflowed to the North Atlantic where they formed a deep water mass (Howe et al.,  
439 2016; Keigwin and Swift, 2017). The classical view of Nordic Sea behaviour during cold  
440 periods is that freshwater from melting ice-sheets and -bergs suppresses convection  
441 resulting in a severe reduction or even cessation of the AMOC inflow and overflow (e.g.  
442 a recent model, including consideration of the EGC, analysing this is from Liu et al,  
443 (2018)). However an emerging view is of a slowdown (not cessation) of Nordic Sea  
444 overflows in cold periods (Howe et al., 2016; Keigwin and Swift, 2017). A very recent  
445 view is that ice discharges in the North Pacific precede Heinrich events and may be

446 implicated as a triggering mechanism (Walczuk et al., 2020). In the Nordic Seas Atlantic  
447 water inflow persisted throughout the Pleistocene glacials over the Norwegian slope  
448 (Sarnthein et al., 1994; Newton et al., 2018). The evidence here indicates a persistent  
449 outflow along the N Iceland Slope with reductions during HS H- events 1, 4, and 6. Flow  
450 speed decreases have been noted for both shallow and deep flows in this region during  
451 stadials and glacial intervals of the late and mid-Quaternary (Kleiven et al., 2011;  
452 McCave and Andrews, 2019b). The Younger Dryas often shows speed decreases but  
453 some cores record increased flow (McCave and Andrews, 2019b), as is seen here. These  
454 disparities remain a puzzle.

455

456 *4.2 Rationalizing mineralogical and biomarker proxies for sea ice reconstruction* When  
457 detected, the concentrations of IP<sub>25</sub> and HBI II were mainly much lower than those  
458 reported previously for mid-late Holocene (ca. 6-0 cal. ka) and deglacial (ca. 15-11 ka)  
459 sites from the NIS (Cabedo-Sanz et al., 2016; Xiao et al., 2017). However, the presence  
460 and concentration of IP<sub>25</sub> at ca. 3.7 ka aligns with previous data reported from core  
461 JR51GC35 (located 76 km SW of #2274 (Figs.1B and 7; Table 1)) for the mid-Holocene  
462 (Cabedo-Sanz et al., 2016), consistent with the delivery of drift ice across the NIS at that  
463 time (Fig. 7). The otherwise general absence of IP<sub>25</sub> and HBI II in #2274 points towards  
464 an environment unfavorable for sea ice diatom growth, namely ice-free conditions or a  
465 setting of near-permanent ice cover. To distinguish between these two scenarios, we  
466 measured three other biomarker types indicative of open water conditions, i.e.  
467 brassicasterol, HBI III and alkenones. In the case of brassicasterol, a phytosterol  
468 characteristic of marine diatoms (Volkman, 1986), concentrations in selected sediments

469 from #2274 were relatively high in the Holocene section and typically two orders of  
470 magnitude lower in older (>14 ka) intervals, indicative of much lower glacial primary  
471 productivity reflecting near-perennial sea ice cover. Similarly, HBI III, a biomarker  
472 derived from certain open water diatoms (Belt et al., 2017), was only detected in  
473 Holocene sections (data not shown). Consistent with these findings, concentrations of  
474 alkenones derived from coccolithophorid blooming in mid-late summers were also  
475 substantially lower in the older sections compared to those in the Holocene (Fig. 6).  
476 Further, the relatively high percentage contribution of the tetra-unsaturated alkenone  
477 C<sub>37:4</sub> prior to the Holocene (mean value 36% compared to 6% for the Holocene) is  
478 consistent with a dominance of polar waters (Sicre et al., 2002; Bendle et al., 2005)  
479 potentially laden with sea ice. Alkenone-derived SST estimates for the Holocene (ca. 7–  
480 9°C) are in line with those reported from other high-resolution studies from the NIS (e.g.  
481 Bendle and Rosell-Melé, 2007; Sicre et al., 2008b; Kristjansdottir et al. 2016). In  
482 contrast, SST estimates prior to the Holocene were somewhat higher (ca. 8–16°C; mean  
483 11.4°C) although the accuracy of such estimates might be lower than for the Holocene  
484 owing to the relatively high contributions from C<sub>37:4</sub> (Bendle and Rosell-Melé, 2004).  
485 Anomalously warm SSTs associated with low alkenone concentrations during glacial  
486 time have been reported in previous studies and attributed to advection of detrital  
487 alkenones (Sicre et al., 2005; Knutz et al., 2011). Such advection by surface currents can  
488 introduce significant bias in regions where there are large productivity and SST  
489 gradients, thereby overprinting any local signal (Bendle and Rosell-Melé, 2004; Conte et  
490 al., 2006). With extremely low alkenone production due to the presence of ice at #2274,  
491 transport of allochthonous alkenones within the IC likely explains the deviation in SSTs

492 towards seemingly unrealistic warmer values. In any case, the most robust aspects of the  
493 biomarker data  
494 point towards near-perennial sea ice cover prior to the Holocene, although the presence of  
495 both phytosterols and alkenones (albeit at low concentrations) indicates the occurrence of  
496 at least partial open water conditions, potentially restricted to leads or regions of partial  
497 ice melt within otherwise heavily consolidated pack ice. Such conditions would likely  
498 have led to short-term and reduced primary production during relatively short summer  
499 seasons and limited to the near-surface layer due to a strongly-stratified water column  
500 resulting from partial ice melt. Both such uppermost surface layer production conditions  
501 in leads and advection of allochthonous alkenones within the IC would account for the  
502 anomalously high glacial SSTs.

503         Our conclusion of near-perennial sea ice during MIS 3 and MIS 2 is broadly  
504 consistent with outcomes from a recent 120,000 yr reconstruction of sea-ice conditions  
505 for the North Atlantic (Maffezzoli et al., 2019) based on the analysis of enriched bromine  
506 ( $Br_{enr}$ ) in an ice core from the Renland Ice Cap (RIC) 560 km WNW from #2274 (Figs. 1  
507 and 7 [RIC]). Albeit at a much broader spatial resolution (i.e. 50-85° N), Maffezzoli et al.  
508 (2019) proposed that MIS 3 and MIS 2 experienced a (variable) mix of multi-year and  
509 first-year sea ice, before transitioning to mainly first-year ice and open water conditions  
510 following the termination of the LGM. Interestingly, the greater range of sea ice cover  
511 inferred from the RIC  $Br_{enr}$  record is not at all clear in our #2274 record, but is evident in  
512 a biomarker record from the eastern Nordic Seas, with extensive/near-perennial sea ice  
513 cover during stadials and H-events (i.e. comparable to #2274) but ice-free conditions

514 during interstadials (since ca. 90 ka BP); such differences between marine sites in the  
515 western and eastern Nordic Seas presumably reflects the variable influence of warm  
516 Atlantic water, limited to the eastern Nordic Seas (Hoff et al., 2016). Such regional  
517 differences are also evident from a more recent biomarker study in the eastern Nordic Seas,  
518 with significant reductions (increases) to sea ice extent during Greenland Interstadials  
519 (Stadials) between ca. 41 and 32 ka (Sadatzki et al., 2020). The most prominent signature  
520 of first-year ice in the  $Br_{enr}$  records occurred during the Younger Dryas and it is noteworthy  
521 that a transition from permanent to increasing seasonal sea ice at the NIS was reported for  
522 this interval following a biomarker-based reconstruction of surface oceanographic  
523 conditions from core #2272 (Fig. 1; 7; Xiao et al., 2017). Further, based on relatively high  
524 concentrations of  $IP_{25}$  in MD99-2272 during the Younger Dryas and the preceding Bølling-  
525 Allerød, Xiao et al. (2017) concluded that biomarker production was likely associated with  
526 locally formed first year ice rather than from advected drift ice, the latter being a feature of  
527 modern-day oceanography. In contrast, our new data from #2274 indicate still near-  
528 permanent sea ice cover at this time (Fig. 7). As such, we interpret the combined ice core  
529 and marine sediment core data to suggest that as climate conditions ameliorated at the end  
530 of the LGM, near-permanent sea ice cover transitioned to first-year seasonal sea ice in the  
531 southern part of the region, especially during the Bølling-Allerød and Younger Dryas,  
532 likely due to increasing influence of the IC (Xiao et al., 2017); however, the spatial extent  
533 of this area of first year ice, located southward of the near-permanent sea ice front that  
534 characterizes MIS 3 and MIS 2, remains uncertain at this point (see Fig. 7 sub-panel).  
535 Large-scale sea ice reduction then characterized the early Holocene (Fig. 7), with a marked  
536 increase in all open water primary productivity biomarker proxies (Fig. 6). Increasing drift



537 ice subsequently became a characteristic of the NIS from the mid Holocene onwards (Fig.  
538 7; Cabedo-Sanz et al., 2016).

### 539 **Conclusions**

540 The multi-proxy sediment data from core #2274 130 km off the north Iceland coast  
541 appears at first sight to yield conflicting interpretations depending on whether sediment  
542 mineral composition or biomarker proxy data are being considered; however, these can  
543 be resolved through a more detailed consideration of the mode(s) of iceberg drift and  
544 trajectory through largely consolidated and near-pervasive sea ice. The low- resolution  
545 sampling for grain-size restricts detailed interpretation but the sediments are mostly  
546 moderately sorted in the silt range allowing a valid record of bottom flow speed. This  
547 shows low flow speeds during H-events 1, 4 and 6 related to decrease in Nordic Sea  
548 overflow, but not cessation, and a peak in the Younger Dryas.

549 The mineral composition of the < 2 mm grain-size sediment samples shows 5  
550 peaks with wt% of quartz values significantly higher than Holocene values. The  
551 variations in the quartz wt% are also reflected in the estimated contributions of sediment  
552 from Precambrian and Caledonian bedrock sources of NE Greenland. These data require  
553 sediment transport to the #2274 site during MIS 3 and MIS 2. If the transport is by  
554 icebergs then the sea ice cover had to allow icebergs to drift southward, as they do at  
555 present (Figs. 1C, 7). A framework of near-permanent sea ice is confirmed from ultra-low  
556 seasonal sea ice and open water biomarker concentrations. On the other hand, the  
557 occurrence of non-zero concentrations of some phytoplanktic biomarkers, and numbers of  
558 near-surface planktonic foraminifera (Table 3) points to some short-term open water

559 conditions, either from limited sea ice melt or following the opening of leads; the  
560 presence of drifting icebergs may be significant in this respect (Fig. 7).

561 An underlying question for HS H-events is whether North Atlantic-wide glacial  
562 marine sediment events were triggered as a response to events in Hudson Strait or  
563 whether the events are part of a shared response to broader regional oceanographic  
564 conditions (e.g. Marcott, et al., 2011; Bassis et al., 2017; Velay-Vitow et al.,  
565 2019). Thus, were “coeval” HS H- events on the East Greenland margin (Stein et al.,  
566 1996; Andrews et al., 1998; Voelker, 1999), or lagged events (e.g. Baffin Bay: Simon et  
567 al., 2014 Jennings et al., 2018), triggered in response to events in the Hudson Strait ice  
568 stream? If our quartz and IRD events (Figs. 3 and 8) are indeed coeval with HS H-  
569 events, this implies that the stability of ice streams on the NE and E Greenland shelf (and  
570 N Iceland) and Hudson Strait may all have been affected by basin-wide subsurface  
571 warming in response to a reduction in the Atlantic meridional overturning circulation  
572 (Shaffer et al., 2004; Clark et al., 2007; Marcott et al., 2011).

573

#### 574 **Acknowledgements**

575 We thank Dr Anne E. Jennings for picking and providing the foraminifera for the  
576 radiocarbon dates, and Dr Haflidi Haflidasson for the identification and geochemical  
577 analysis of the tephra. Professor Grant Bigg provided guidance on the role of icebergs  
578 and sea ice. We thank the Centre National de la Recherche Scientifique (CNRS) for  
579 MAS salary and the crew of the *RV Marion Dufresne* for coring operations during the  
580 IMAGESV cruise. Data from this study will be archived at: [www.Pangaea.de](http://www.Pangaea.de), along with  
581 other IMAGESV data for MD99-2274. We acknowledge the availability and our use of

582 data from PS1726, PS1730, and PS2644, which we accessed through [www.Pangaea.de](http://www.Pangaea.de).

583 Finally, we thank three anonymous reviewers who provided critical

584 and helpful feedback on previous versions of the manuscript.

#### 585 **Tables**

586 Table 1 Location of the cores referenced in this study and showing distance from

587 MD992274. Cores located on Fig. 1A and B unless noted as NA. The last 5 sites are

588 cores that specify sediment sources based on radiogenic isotopic data (Verplanck et al.,

589 2009; White et al., 2016).

590

591 Table 2 A and B: Data for two possible depth/age models for MD99-2274 used in the

592 Bayesian “Bacon” model—see text.  $cc = 0$  when date derived from other sources and

593 does not require calibration;  $cc = 2$  when ocean reservoir correction  $DR = 0$  is used

594 (marine IntelCal 13; Reimer et al., 2013).

595

596 Table 3: Depth/age data and calibrated ages for radiocarbon dates on near-surface

597 planktonic foraminifera (see Figs. 1 and 5). Ocean reservoir correction  $DR = 0$ .

598

599 **Suppl. Table:** Geochemistry of the tephra layer (see text). Courtesy Dr. H. Haflidasson)

600

#### 601 **Figure Captions**

602 Figure 1: A) location of MD99-2274 and some other cores noted in the paper (Table 1)

603 (ODV, Schlitzer, 2011). The shaded areas represent the late glacial maximum (LGM)

604 extent of the ice sheets north of Denmark Strait; the words “basalt” and “felsic” define

605 the primary sediment mineral sources and the arrows show probable flow paths for  
606 icebergs. BB = Blossville Basi; TMF = Scoresby Sund Trough Mouth Fan; B)  
607 Additional cores referenced in the paper (see also Table 1). Note that “Cald” on this  
608 figure references the southern outcrop of the Greenland Caledonides (Higgins et al.,  
609 2008). SS = Scoresby Sund; RIC = Renland Ice Cap. C) Surface and bottom currents and  
610 historical April sea-ice edge (1870-1920) (dashed white line; Divine and Dick, 2006).  
611 NIIC = North Iceland Irminger Current; EGC = East Greenland Current; EIC = East  
612 Iceland Current; Yellow lines: Bottom Currents DSOW = Denmark Strait Overflow  
613 Water; NIJ = North Iceland Jet., S = Separated East Greenland Current; OC = Iceland Sea  
614 Ocean Convection site (after Harden et al., 2016).

615

616 Figure 2: A) Downcore plot of magnetic susceptibility ( $SI^{-5}$ ) and Bayesian ((Blaauw and  
617 Christen, 2016) depth age plots for MD99-2274 (see Table 2)---the red curve is for the  
618 initial available data blue curve is for the estimated ages with the addition of an estimated  
619 core top age and the presence of the Vedde and NAAZII tephras (see text). The Marine  
620 Isotope Stage (MIS) boundaries are indicated. Location of radiocarbon dates and tephras  
621 are noted. B) Plot of the departures from the median values of magnetic susceptibility  
622 ( $2.03 * 10^{-3} SI$ ) and quartz wt% (5.3). Note that the quartz axis is reversed.

623

624 Figure 3: Variation in the Sortable Silt mean size (3-point 1-2-1 weighted smoothing with  
625 raw data dots) and IRD%  $>240 \mu m$ . Minima in  $\overline{SS}$  are seen at the time of Hudson Strait H  
626 events -H6, -H4 and -H1 while -H4, -H2, early -H1 and the YD (-H0) are marked by

627 elevated IRD %. Blue bars are regions where the data are unreliable indicators of flow  
628 speed according to the  $\overline{SS}$  -SS% correlation criterion of McCave and Andrews, (2019a)

629

630 Figure 4: Plots of the variations in the weight% of minerals in MD99-2274, the  
631 quartz/pyroxene ratio, and magnetic susceptibility. The green shaded areas represent  
632 Holocene values, hence points above represent departures. Numbers 1 through 5 identify  
633 IRD quartz peaks. The vertical blue shading areas represent times when the weight% of  
634 quartz exceeds Holocene limits.

635

636 Figure 5: Plots of the sediment source percentages and the degree of fit (DOF), that is the  
637 average absolute bias in the SedUnMix calculation of (observed mineral wt% - predicted  
638 mineral weight%) for each sample. The top panel shows the location of measurable  
639 quantities of gravel, and sites of tephra layers and the radiocarbon dates on near-surface  
640 planktonic foraminifera (Table 3). Numbers on the NE Greenland panel represent the  
641 peaks in that source and the yellow bars locate areas with minimal input from that area.

642

643 Figure 6: Biomarker data (A) IP<sub>25</sub> and HBI II concentrations; (B)  $\sum C_{37:3} + C_{37:2}$  alkenone  
644 and brassicasterol concentrations; C) SST° C estimates and the %C<sub>37:4</sub>; and D) Weight %  
645 quartz and different coarse sediment fractions.

646

647 Figure 7: Schematic presentation of changes in sea ice and iceberg distribution. The first  
648 panel (upper left) shows core locations (see Table 1 and Fig. 1A and B) and the adjoining  
649 panel the inferred conditions during MIS 3 and 2 with pervasive sea ice and embedded  
650 icebergs. The remaining panels show the proposed evolution in the state of sea ice and

651 iceberg supply (red triangles) during deglaciation into the Holocene (adapted from  
652 Cabedo-Sanz et al., 2016; Xiao et al., 2017). SS =Scoresby Sound, RIC=Renland Ice  
653 Cap.

654

655

656 Figure 8: Analysis of the quartz wt% records from PS2644 (Vogt, 2017) and MD99-2274  
657 at a common 0.6 ky spacing. A) Original quartz data (black line) and the wavelet  
658 reconstructions for the two records; B) Cross-wavelet power spectrum of quartz wt% for  
659 PS2644 and MD99-2274. The cone of confidence indicated by the light grey areas;  
660 0.05% probability area demarcated by white line. Arrows pointing to the right mean that  
661 the two records are in phase, arrows pointing down mean that x leads y, arrows pointing  
662 to the left indicate the records are anti-phase and pointing up indicates that #2274 leads  
663 PS2644. C) Cross-wavelet (Fig. 8B) average power. The 0.05 significance period is red  
664 and delimited by the dashed slanting line. The horizontal dashed line indicates the peak  
665 periodicity (~8.5 ky).

666

667

668 Suppl. Figure 1: Data for VM30-130 (see Fig. 1 and Table 3).

669

670 Suppl. Figure 2: Showing the reduced major axis association between sortable silt mean  
671 size ( $\overline{SS}$ ) and SS%.

672

673 Suppl. Figure 3:  $d^{18}O$  *N. pachyderma* plots of cores from the Blosseville Basin/Scoresby  
674 Sund Trough Mouth Fan (see Fig. 1 and 8) from cores PS1730 (Stein et al., 1996a,b,  
675 and PS2644 (Voelker, 1999).

676 References

677 Aitchison, J., 1986. The statistical analysis of compositional data. Chapman and Hall,  
678 London.

679 Andrews, J.T., Bjork, A.A., Eberl, D.D., Jennings, A.E., Verplanck, E.P., 2015.

680 Significant differences in late Quaternary bedrock erosion and transportation: East  
681 versus West Greenland  $\sim 70^\circ N$  and the evolution of glacial landscapes. *Journal of*  
682 *Quaternary Science* 30, 452-463.

683 Andrews, J.T., Cabedo-Sanz, P., Jennings, A.E., Olafsdottir, S., Belt, S.T., Geirsdottir,  
684 A., 2018. Sea ice, ice-rafting, and ocean climate across Denmark Strait during rapid  
685 deglaciation (similar to 16-12 cal ka BP) of the Iceland and East Greenland shelves.  
686 *Journal of Quaternary Science* 33, 112-130.

687 Andrews, J.T., Cooper, T.A., Jennings, A.E., Stein, A.B., Erlenkeuser, H., 1998: Late  
688 Quaternary iceberg-rafted detritus events on the Denmark Strait–Southeast  
689 Greenland continental slope ( $\sim 65^\circ N$ ): related to North Atlantic Heinrich events?  
690 *Marine Geology* 149, 211-228.

691 Andrews, J.T., Dunhill, G., Vogt, C., Voelker, A.H.L., 2017. Denmark Strait during the  
692 Late Glacial Maximum and Marine Isotope Stage 3: Sediment sources and transport  
693 processes. *Marine Geology* 390, 181-198.

694 Andrews, J.T., Eberl, D.D., 2007. Quantitative mineralogy of surface sediments on the  
695 Iceland shelf, and application to down-core studies of Holocene ice-rafted sediments.  
696 *Journal of Sedimentary Research* 77, 469-479.

697 Andrews, J.T., Eberl, D.D., 2012. Determination of sediment provenance by unmixing  
698 the mineralogy of source-area sediments: The "SedUnMix" program. *Marine*  
699 *Geology* 291, 24-33.

700 Andrews, J.T., Helgadottir, G., 2003. Late Quaternary ice cap extent and deglaciation of  
701 Hunafloall, NorthWest Iceland: Evidence from marine cores. *Arctic, Antarctic, and*  
702 *Alpine Research* 35, 218-232.

- 703 Andrews, J.T., Jónsdóttir, I., Geirsdóttir, A., 2019. Tracking Holocene drift-ice limits on  
704 the NW/SW Iceland shelf: comparing proxy data with observation and historical  
705 evidence. *Arctic, Antarctic, and Alpine Research*. 51, 96-114.
- 706 Andrews, J.T., Kristjansdóttir, G.B., Eberl, D.D., Jennings, A.E., 2013. A quantitative  
707 X-ray diffraction inventory of tephra and volcanic glass inputs into the Holocene  
708 marine sediment archives of Iceland: A contribution to V.A.S.T. *Polar Research* 1-  
709 15.
- 710 Andrews, J.T., Stein, R., Moros, M., Perner, K., 2016. Late Quaternary changes in  
711 sediment composition on the NE Greenland margin (~73 degrees N) with a focus on  
712 the fjords and shelf. *Boreas* 45, 381–397.
- 713 Andrews, J.T., Voelker, A., 2018. "Heinrich events" (& sediments): A history of  
714 terminology and recommendations for future usage. *Quaternary Science Reviews*  
715 187, 31-40.
- 716 Andrews, J.T., Vogt, C., 2014. Source to Sink: Statistical identification of regional  
717 variations in the mineralogy of surface sediments in the western Nordic Seas (58°N –  
718 75°N; 10° W -- 40°W). *Marine Geology* 357, 151-162.
- 719 Andrews, J.T., Vogt, C., 2020a. Variations in felsic- versus mafic-sources in the Western  
720 Nordic Seas during MIS 1 to MIS 4 *Marine Geology* 424, 106164.
- 721 Andrews, J.T. and Vogt, C. 2020b: Results of bulk sediment X-ray diffraction analysis and  
722 quantification of mineral phases based on the RockJock quantitative analysis. *Pangaea*.  
723 <https://doi.pangaea.de/10.1594/PANGAEA.923135>
- 724 Austin, W.E.N., Hibbert, F.D., 2012. Tracing time in the ocean: a brief review of  
725 chronological constraints (60-8 kyr) on North Atlantic marine event-based  
726 stratigraphies. *Quaternary Science Reviews* 36, 28-37.
- 727 Bai, Y., Chen, J.F., Sicre, M.-A., Jin, H., Ren, J., Li, H., Xue, B., Ji, Z., Zhuang, Y.,  
728 Klein, V., Zhao, M., 2019. Seasonal and spatial variability of sea ice and  
729 phytoplankton biomarker flux in the Chukchi Sea (Western Arctic). *Progress in*  
730 *Oceanography* 171, 22-37.
- 731 Bassis, J.N., Petersen, S.V. Cathles, L.M., 2017. Heinrich events triggered by ocean  
732 forcing and modulated by isostatic adjustment. *Nature* 542, 332-334.



- 733 Belt, S.T., 2018. Source-specific biomarkers as proxies for Arctic and Antarctic sea ice,  
734 Organic Geochemistry 125, 277–298, doi: 10.1016/j.orggeochem.2018.10.002.
- 735 Belt, S.T., Masse, G., Rowland, S.J., Poulin, M., Michel, C., LeBlanc, B., 2007. A novel  
736 chemical fossil of palaeo sea ice: IP<sub>25</sub>. Organic Gechemistry 38, 16-27.
- 737 Belt, S.T., Müller, J., 2013. The Arctic sea ice biomarker IP<sub>25</sub>: a review of current  
738 understanding, recommendations for future research and applications in palaeo sea  
739 ice reconstructions. Quaternary Science Reviews 79, 9-25.
- 740
- 741 Belt, S.T., Cabedo-Sanz, P., Smik, L., Navarro-Rodriguez, A., Berben, S.M. P., Knies, J.,  
742 Husum, K., 2015. Identification of paleo Arctic winter sea ice limits and the marginal  
743 ice zone: optimised biomarker-based reconstructions of late Quaternary Arctic sea  
744 ice. Earth and Planetary Science Letters 431, 127-139.
- 745 Belt, S.T., Brown, T.A., Smik, L., Tatarek, A., Wiktor, J., Stowasser, G., Assmy, P.,  
746 Allen, C.A., Husum, K., 2017. Identification of C<sub>25</sub> highly branched isoprenoid  
747 (HBI) alkenes in diatoms of the genus *Rhizosolenia* in polar and non-polar marine  
748 phytoplankton. Organic Geochemistry 110, 65–72
- 749 Bendle, J., Rosell-Melé, A., 2004. Distributions of UK'<sub>37</sub> and UK<sub>37</sub> in the surface waters  
750 and sediments of the Nordic Seas: implications for paleoceanography. Geochemistry,  
751 Geophysics, Geosystems, Q11013. doi:10.1029/2004GC000741.
- 752 Bigg, G.R., 2016. Icebergs. Their Science and links to Global Change. Cambridge  
753 University Press.
- 754 Blaauw, M., 2012. Out of tune: the dangers of aligning proxy archives. Quaternary Science  
755 Reviews 36, 38-49.
- 756 Blaauw, M., Christen, J.A., Bacon Manual, 2016. -v2.2, p. 11 pp.
- 757 Blaauw, M., Christen, J.A., 2005. The problems of radiocarbon dating. Science 308,  
758 1552-1553.
- 759 Boers, N., Ghil, M., Rousseau, D.D., 2018. Ocean circulation, ice shelf, and sea ice  
760 interactions explain Dansgaard-Oeschger cycles. Proceedings of the National  
761 Academy of Sciences of the United States of America 115, E11005-E11014.

- 762 Boers, N., Goswami, B., Ghil, M., 2017. A complete representation of uncertainties in  
763 layer-counted paleoclimate archives. *Climate of the Past* 13, doi:10.5194/cp-131169-  
764 2017
- 765 Brakstad, A., Vage, K., Havik, L., Moore, G.W.K., 2019. Water Mass Transformation in the  
766 Greenland Sea during the Period 1986-2016. *Journal of Physical Oceanography* 49,  
767 121140.
- 768 Brendryen, J., Haflidason, H., Sejrup, H.P., 2011. Non-synchronous deposition of North  
769 Atlantic Ash Zone II in Greenland ice cores, and North Atlantic and Norwegian Sea  
770 sediments: an example of complex glacial-stage tephra transport. *Journal of*  
771 *Quaternary Science* 26, 739-745.
- 772 Brooks, C.K., Nielsen, T.F.D., 1982. The Phanerozoic development of the  
773 Kangerdlugssuaq area, East Greenland. *Meddelelser on Gronland, Geoscience* 9, 1-  
774 30.
- 775 Cabedo-Sanz, P., Belt, S.T., Jennings, A.E., Andrews, J.T., Geirsdóttir, Á., 2016.  
776 Variability in drift ice export from the Arctic Ocean to the North Icelandic Shelf over  
777 the last 8000 years: A multi-proxy evaluation. *Quaternary Science Reviews* 146,  
778 99115.
- 779 Chayes, F., 1971. *Ratio correlation*. University of Chicago Press, Chicago.
- 780 Clark, D.L., 1990a. Arctic Ocean ice cover; Geologic history and climatic significance,  
781 *The Geology of North America*. Geological Society of America, pp. 53-62.
- 782 Clark, D.L., 1990b. Stability of the Arctic Ocean ice-cover and Pleistocene warming  
783 events: Outlining the problem, in: Bleil, U., Thiede, J. (Eds.), *Geological History of*  
784 *the Polar Oceans: Arctic Versus Antarctic*. Kluwer Academic Publishers,  
785 Netherlands, pp. 273-287.
- 786 Clark, P. U., Hostetler, S. W., Pisias, N. G., Schmittner, A., and Meissner, K. J., 2007.  
787 Mechanisms for a  $\sim 7$  kyr climate and sea-level oscillation during marine isotope stage  
788 3. In Schmittner, A., Chiang, J., and Hemming, S. (eds.), *Ocean Circulation:*  
789 *Mechanisms and Impacts*. Geophysical Monograph 173. Washington, DC: AGU, pp.  
790 209–246.
- 791 Conte, M. H., M.-A. Sicre, C. Rühlemann, J. C. Weber, S. Schulte, D. Schulz-Bull, T.

- 792 Blanz, 2006. Global temperature calibration of the alkenone unsaturation index  
793 ( $U^{K_{37}}$ ) in surface waters and comparison with surface sediments, *Geochemistry,*  
794 *Geophysics, Geosystems* 7, Q02005, doi:10.1029/2005GC001054.
- 795 Darby, D.A., Andrews, J.T., Belt, S.T., Jennings, A.E., Cabedo-Sanz, P., 2017. Holocene  
796 cyclic records of ice-rafted debris and sea ice variations on the East Greenland and  
797 NW Iceland margins. *Antarctic, Arctic, and Alpine Research* 49, 649-672.
- 798 Darby, D.A., Zimmerman, P., 2008. Ice-rafted detritus events in the Arctic during the last  
799 glacial interval, and the timing of the Innuitian and Laurentide ice sheet calving  
800 events. *Polar Research* 27, 114-127.
- 801 Davies, S.M., Wastegard, S., Rasmussen, T.L., Svensson, A., Johnsen, S.J., Steffensen,  
802 J.P., Andersen, K.K., 2008. Identification of the Fugloyarbanki tephra in the NGRIP  
803 ice core: a key tie-point for marine and ice-core sequences during the last glacial  
804 period. *Quaternary Science Reviews* 23, 409-414.
- 805 Divine, D.V., Dick, C., 2006. Historical variability of the sea ice edge position in the  
806 Nordic Seas. *Journal of Geophysical Research* 111, 14pp.  
807 doi:10.1029/2004JC002851.
- 808 Dokken, T.M., Nisancioglu, K.H., Li, C., Battisti, D.S., Kissel, C., 2013.  
809 Dansgaard-Oeschger cycles: Interactions between ocean and sea ice intrinsic to the  
810 Nordic seas.  
811 *Paleoceanography* 28, 491-502.
- 812 Domack, E.W., Jacobson, E.A., Shipp, S., Anderson, J.B., 1999. Late  
813 Pleistocene-Holocene retreat of the West Antarctic Ice-Sheet system in the Ross Sea:  
814 Part 2 - Sedimentologic and stratigraphic signature. *Geological Society of America*  
815 *Bulletin* 111, 1517-1536.
- 816 Dowdeswell, J.A., Elverhoi, A., Andrews, J.T., Hebbeln, D., 1999. Asynchronous de-  
817 position of ice-rafted layers in the Nordic seas and North Atlantic Ocean. *Nature* 400,  
818 348–351.
- 819 Eberl, D.D., 2003. User guide to RockJock: A program for determining quantitative  
820 mineralogy from X-ray diffraction data. United States Geological Survey, Open File  
821 Report 03-78, 40 pp, Washington, DC.

- 822 Elliot, M., Labeyrie, L., Dokken, T., Manthe, S., 2001. Coherent patterns of ice-rafted  
823 debris deposited in the Nordic regions during the last glacial (10-60 ka). *Earth and*  
824 *Planetary Science Letters* 194, 151–163.
- 825 Evans, J., Dowdeswell, J. A., Grobe, H., Niessen, F., Stein, R., Hubberten, H.-W. &  
826 Whittington, R. J. 2002: Late Quaternary sedimentation in Kaiser Joseph Fjord and  
827 the continental margin of East Greenland. In Dowdeswell, J. A. & O Cofaigh, C.  
828 (eds.): *Glacier-Influenced Sedimentation on High-Latitude Continental Margins*,  
829 *Special Publication 203*, 149–179. The Geological Society of London, London.
- 830 Evans, J., Dowdeswell, J. A., Grobe, H., Niessen, F., Stein, R., Hubberten,  
831 H.-W. & Whittington, R. J. 2002: Late Quaternary sedimentation in  
832 Keiser Joseph Fjord and the continental margin of East Greenland. In  
833 Dowdeswell, J. A. & O Cofaigh, C. (eds.):  
834 *Glacier-Influenced Sedimentation on High-Latitude Continental*  
835 *Margins*, 149–179. The Geological Society of London, *Special*  
836 *Publication 203*, London.
- 837 Evans, J., O Cofaigh, C., Dowdeswell, J. A. & Wadhams, P. 2009:  
838 Marine geophysical evidence for former expansion and flow of the  
839 Greenland Ice Sheet across the north-east Greenland continental shelf.  
840 *Journal of Quaternary Science* 24, 279–293.
- 841 Evans, J., Dowdeswell, J. A., Grobe, H., Niessen, F., Stein, R., Hubberten,  
842 H.-W. & Whittington, R. J. 2002: Late Quaternary sedimentation in Keiser Joseph Fjord and the continental margin of  
843 East Greenland. In Dowdeswell, J. A. & O Cofaigh, C. (eds.):  
844 *Glacier-Influenced Sedimentation on High-Latitude Continental*  
845 *Margins*, 149–179. The Geological Society of London, *Special*  
846 *Publication 203*, London.
- 847 Evans, J., O Cofaigh, C., Dowdeswell, J. A. & Wadhams, P. 2009:  
848 Marine geophysical evidence for former expansion and flow of the  
849 Greenland Ice Sheet across the north-east Greenland continental shelf.  
850 *Journal of Quaternary Science* 24, 279–293.  
851

- 852 Evans, J., Dowdeswell, J. A., Grobe, H., Niessen, F., Stein, R., Hubberten, H.-W. &  
853 Whittington, R. J. 2002: Late Quaternary sedi- mentation in Kejser Joseph Fjord and  
854 the continental margin of East Greenland. In Dowdeswell, J. A. & O Cofaigh, C.  
855 (eds.): Glacier-Influenced Sedimentation on High-Latitude Continental Margins,  
856 149–179. The Geological Society of London, Special Publication 203, London.
- 857 Evans, J., O Cofaigh, C., Dowdeswell, J. A. & Wadhams, P. 2009: Marine geophysical  
858 evidence for former expansion and flow of the Greenland Ice Sheet across the  
859 northeast Greenland continental shelf. *Journal of Quaternary Science* 24, 279–293.
- 860 Funder, S., Goosse, H., Jepsen, H., Kaas, E., Kjaer, K.H., Korsgaard, N.J., Larsen, N.K.,  
861 Linderson, H., Lysa, A., Moller, P., Olsen, J., Willerslev, E., 2011a. A 10,000-year  
862 record of Arctic Ocean sea-ice variability-view from the beach. *Science*, 333,  
863 747750.
- 864 Funder, S., Kjeldsen, K.K., Kjaer, K.H., O Cofaigh, C., 2011b. The Greenland Ice Sheet  
865 during the past 300,000 years: A review. p. 699-713 In, Ehlers, J., Gibbard, P.L., and  
866 Hughes, P.D., (Eds), *Quaternary Glaciations - Extent and Chronology: A Closer*  
867 *Look*. Elsevier, Amsterdam
- 868 Greco, M., Jonkers, L., Kretschmer, K., Bijma, J., Kucera, M., 2019. Depth habitat of the  
869 planktonic foraminifera *Neogloboquadrina pachyderma* in the northern high latitudes  
870 explained by sea-ice and chlorophyll concentrations. *Biogeosciences* 16, 3425-3437.
- 871 Hammer, O, Harper, D.A.T., and Ryan, P.D., 2001. PAST: Paleontological statistics  
872 software package for education and data analysis. *Palaeontological Electronica*,  
873 <http://palaeo-electronica.org>
- 874 Harden, B.E., Pickart, R.S., Valdimarsson, H., Vage, K., de Steur, L., Richards, C., Bahr,  
875 F., Torres, D., Borve, E., Jonsson, S., Macrander, A., Osterhus, S., Havik, L.,  
876 Hattermann, T., 2016. Upstream sources of the Denmark Strait Overflow:  
877 Observations from a high-resolution mooring array. *Deep-Sea Research Part I-*  
878 *Oceanographic Research Papers* 112, 94-112
- 879 Hassani, H., 2007. Singular Spectrum Analysis: Methodology and comparison. *Journal of*  
880 *Data Science* 5, 239-257.
- 881 Heinrich, H., 1988. Origin and consequences of cyclic ice rafting in the Northeast  
882 Atlantic Ocean during the past 130,000 years. *Quaternary Research* 29, 143-152.

- 883 Hemming, S.R., 2004. Heinrich Events: Massive late Pleistocene detritus layers of the  
884 North Atlantic and their global climate imprint. *Reviews of Geophysics* 42,  
885 RG1005/2004.
- 886 Henriksen, H., 2008. Geological history of Greenland. Geological Survey of Denmark  
887 and Greenland, Copenhagen.
- 888 Hesse, R., 2016. Ice-proximal Labrador Sea Heinrich layers: a sedimentological  
889 approach. *Canadian Journal of Earth Sciences* 53, 71-100.
- 890 Higgins, A.K., Gilotti, J.A., Smith, P.M., 2008. The Greenland Caledonides. Evolution of  
891 the Northeast margin of Laurentia. Geological Society of America, Boulder, CO, p.  
892 368.
- 893 Hoff, U., Rasmussen, T.L., Stein, R., Ezat, M.M., Fahl, K., 2016. Sea ice and  
894 millennial-scale climate variability in the Nordic seas 90 kyr ago to present. *Nature*  
895 *Communications* 7. 12247.
- 896 Howe, J.N.W., Piotrowski, A.M., Noble, T.L., Mulitza, S., Chiessi, C.M., Bayon, G.,  
897 2016. North Atlantic Deep Water production during the Last Glacial Maximum.  
898 *Nature Commun.* 7, 11765. doi: 10.1038/ncomms11765
- 899 Jennings, A.E., Andrews, J.T. et al., 2018. Baffin Bay paleoenvironments in the LGM  
900 and HS1: Resolving the ice-shelf question. *Marine Geology*. 402, 5-16.
- 901 Jennings, A.E., Reilly, B., Andrews, J.T., Hogen, K., Walczak, M., Stoner, J., Mix, A.C.,  
902 Jakobsson, M., 2019. Modern ice shelf facies and Early Holocene counterparts in  
903 Petermann Fjord and Northern Nares Strait, International Association Sedimentology  
904 IAS, Rome.
- 905 Jonsson, S., and Valdimarsson, H. 2004. A new path for the Denmark Strait overflow  
906 water from the Iceland Sea to Denmark Strait. *Geophysical Research Letters* 31, 4pp.  
907 doi:10.1029/2003GL019214, 012004.
- 908 Jonsson, S., Valdimarsson, H., 2005. The flow of Atlantic water to the North Icelandic  
909 Shelf and its relation to the drift of cod larvae. *ICES Journal of Marine Science* 62,  
910 1350-1359.
- 911 Jonsson, S., Briem, J., 2003. Flow of Atlantic water west of Iceland and onto the north  
912 Atlantic shelf. *ICES Marine Science Symposia* 219, 326-328.

- 913 Keigwin, L.D., and Swift, S.A., 2017. Carbon isotope evidence for a northern source of  
914 deep water in the glacial western North Atlantic. *Proceedings of the National*  
915 *Academy of Sciences of the United States of America* 114, 2831-2835.
- 916 Knudsen, K.-L., Eiriksson, J., 2002. Application of tephrochronology to the timing and  
917 correlation of palaeoceanographic events recorded in Holocene and Late Glacial  
918 shelf sediments off North Iceland. *Marine Geology* 191, 165-188.
- 919 Konert, M., Vandenberghe, J., 1997. Comparison of laser grain size analysis with pipette  
920 and sieve analysis: a solution for the underestimation of the clay fraction.  
921 *Sedimentology* 44, 523-535.
- 922 Knudsen, K.-L., Jiang, D., Jansen, E., Eiriksson, J., Heinemeier, J., Seidenkrantz, M.-S.,  
923 2003. Environmental changes off North Iceland during the deglaciation and the  
924 Holocene: foraminifera, diatoms and stable isotopes. *Marine Micropaleontology* 953,  
925 1-33.
- 926 Knutz, P.C., H. Ebbesen, S. Christiansen, M.-A. Sicre, and A. Kuijpers, 2011. The triple  
927 stage deglacial retreat of the southern Greenland Ice Sheet driven steps by vigorous  
928 Irminger Current, and its significance for the Younger Dryas cooling,  
929 *Paleoceanography*, 26, PA3204, doi:10.1029/2010PA002053, 2011
- 930 Kristjansdottir, G.B., Stoner, J.S., Gronvold, K., Andrews, J.T., Jennings, A.E., 2007.  
931 Geochemistry of Holocene cryptotephra from the North Iceland Shelf (MD992269):  
932 Intercalibration with radiocarbon and paleomagnetic chronostratigraphies.  
933 *The Holocene* 17, 155-176.
- 934 Kristjansson, L., Saemundsson, K., Thorarinsson, S., Saemundsson, K., Thorarinsson, S.,  
935 Einarsson, P., Bjornsson, S., Simonarson, L., Fridleifsson, I., Jaksoisson, S.P.,  
936 Bjornsson, H., 1979. Special Issue: Geology of Iceland. *Jökull* 29, 1-101.
- 937 Labeyrie, L., Jansen, E., Cortijo, E., 2003. Les rapports de campagnes a la mer  
938 MD114/IMAGES V. Institut Polaire Francais Paul-Emile Victor, Brest.
- 939
- 940 Labeyrie, L.D. and Cortijo, E. 2005: Physical properties of sediment core MD99-2274.  
941 *Pangaea*. <https://doi.org/10.1594/PANGAEA.253605>

- 942 Lakeman, T.R., Pienkowski, A.J., Nixon, F.C., Furze, M.F.A., Blasco, S., Andrews, J.T.,  
943 King, E.L., 2018. Collapse of a marine-based ice stream during the early Younger  
944 Dryas chronozone, western Canadian Arctic. *Geology* 46, 211-214.
- 945 Larsen, N.K., Levy, L.B., Carlson, A.E., Buizert, C., Olsen, J., Strunk, A., Bjork, A.A. and Skov,  
946 D.S. (2018) Instability of the Northeast Greenland Ice Stream over the last 45,000 years.  
947 *Nature Communications*, 9.doi: 10.1038/s41467-018-04312-7
- 948 Lind, E.W., Lilja, C., Wastegard, S., Pearce, N.J.G., 2016. Revisiting the Borrobol  
949 Tephra. *Boreas* 45, 693-643.
- 950 Liu, Y., Hallberg, R., Sergienko, O., Samuels, B.L., Harrison, M., & Oppenheimer, M.  
951 2018. Climate response to the meltwater runoff from Greenland ice sheet: evolving  
952 sensitivity to discharging locations. *Climate Dynamics*, 51, 1733–1751. doi  
953 10.1007/s00382-017-3980-7
- 954 Lohne, O.S., Mangerud, J., Birks, H.H., 2013. Precise C-14 ages of the Vedde and  
955 Saksunarvatn ashes and the Younger Dryas boundaries from western Norway and  
956 their comparison with the Greenland Ice Core (GICC05) chronology. *Journal of*  
957 *Quaternary Science* 28, 490-500.
- 958 Maffezzoli, N., Vallelonga, P., Edwards, R., Saiz-Lopez, A., Turetta, C., Kjaer, H.A.,  
959 Barbante, C., Vinther, B., Spolaor, A., 2019. A 120 000-year record of sea ice in the  
960 North Atlantic? *Climate of the Past* 15, 2031-2051.
- 961 Manley, W.F., Jennings, A.E., 1996. Radiocarbon Date List VIII: Eastern Canadian  
962 Arctic, Labrador, Northern Quebec, East Greenland Shelf, Iceland Shelf, and  
963 Antarctica. INSTAAR, University of Colorado, p. 163 pp.
- 964 Marcott, S.A., Clark, P.U., Padman, L., Klinkhammer, G.P., Springer, S.R. , Liu, Z., , Otto-  
965 Bliesner, B.L., Carlson, A.E., Ungerer, A., Padman, J., He, F., Cheng, J. and  
966 Schmittner, A., 2011: Ice-shelf collapse from subsurface warming as a trigger for  
967 Heinrich events. *Proceedings of the National Academy of Sciences of the United*  
968 *States of America* 108, 13415-13419
- 969 Marshall, N.R., Piper, D.J.W., Saint-Ange, F., Campbell, D.C., 2014. Late Quaternary  
970 history of contourite drifts and variations in Labrador Current flow, Flemish Pass,  
971 offshore eastern Canada. *Geology Marine Letters* 34, 457-470.  
972 doi:10.1007/s00367014-0377-z.



- 973 Mauritzen, C., 1996. Production of dense overflow waters feeding the North Atlantic  
974 across the Greenland-Scotland Ridge. 1. Evidence for a revised circulation scheme.  
975 Deep-Sea Research I 43, 769-806.
- 976 Massé, G., Rowland, S.J., Sicre, M.-A., Jacob, J., Jansen, E., Belt, S.T., 2008. Abrupt  
977 climate changes for Iceland during the last millennium: Evidence from high resolution  
978 sea ice reconstructions. Earth and Planetary Science Letters 269, 565–569. Matthews,  
979 I.P., Birks, H.H., Bourne, A.J., Brooks, S.J., Lowe, J.J., Macleod, A., PyneO'Donnell,  
980 S.D.F., 2011. New age estimates and climatostratigraphic correlations for  
981 the Borrobol and Penifiler Tephra: evidence from Abernethy Forest, Scotland.  
982 Journal of Quaternary Science 26, 247-252.
- 983 McCave, I.N., Andrews, J.T., 2019a. Distinguishing current effects in sediments  
984 delivered to the ocean by ice. I. Principles, methods and examples. Quaternary  
985 Science Reviews 212, 92-107.
- 986 McCave, I.N., Andrews, J.T., 2019b. Distinguishing current effects in sediments  
987 delivered to the ocean by ice. II. Glacial to Holocene changes in North Atlantic high  
988 latitude upper ocean flows. Quaternary Science Reviews 223, no. 105902, 21pp.
- 989 McCave, I.N., Hall, I.R., Bianchi, G.G., 2006. Laser vs settling velocity differences in silt  
990 grain-size measurements: estimation of palaeocurrent vigour. Sedimentology 53,  
991 919-928.
- 992 McCave, I.N., Manighetti, B. and Robinson, S.G., 1995. Sortable silt and fine sediment  
993 size/composition slicing: parameters for palaeocurrent speed and palaeoceanography.  
994 Paleoceanography 10, 593-610.
- 995 McCave, I.N., Thornalley, D.J.R., Hall, I.R., 2017. Relation of sortable silt grain-size to  
996 deep-sea current speeds: Calibration of the 'Mud Current Meter'. Deep-Sea Research  
997 Part I 127, 1-12.
- 998 McCave, I.N., Syvitski, J.P.M., 1991. Principles and methods of geological particle size  
999 analysis, in: Syvitski, J.P.M. (Ed.), Principles, methods and application of particle  
1000 size analysis. Cambridge University Press, pp. 3-21.
- 1001 McKay, R., Golledge, N.R., Maas, S., Naish, T., Levy, R., Dunbar, G., Kuhn, G., 2016.  
1002 Antarctic marine ice-sheet retreat in the Ross Sea during the early Holocene.  
1003 Geology 44, 7-10.

- 1004 Millo, C., Sarnthein, M., Erlenkeuser, H., Frederichs, T., 2005. Methane-driven Late  
1005 Pleistocene delta C-13 minima and overflow reversals in the southwestern Greenland Sea.  
1006 *Geology* 33, 873–876.
- 1007 Moles, J.D., McGarvie, D., Stevenson, J.A., Sherlock, S.C., Abbott, P.M., Jenner, F.E.,  
1008 Halton, A.M., 2019. Widespread tephra dispersal and ignimbrite emplacement from a  
1009 subglacial volcano (Torfajökull, Iceland). *Geology* 47, 577-580.
- 1010 Moros, M., McManus, J., Rasmussen, T., Kuijpers, A., Dokken, T., Snowball, I., Nielsen,  
1011 T., Jansen, E., 2004. Quartz content and the quartz-to-plagioclase ratio determined  
1012 by X-ray diffraction: a proxy for ice rafting in the northern North Atlantic? *Earth and*  
1013 *Planetary Science Letters* 218, 389-401.
- 1014 Newton, A.M.W., Huuse, M., and Brocklehurst, S.H. 2018. A persistent Norwegian  
1015 Atlantic Current through the Pleistocene glacials. *Geophysical Research Letters* 45,  
1016 5599–5608. <https://doi.org/10.1029/2018GL077819>
- 1017 Nam, S.-I., Stein, R., Grobe, H., Hubberten, H., 1995. Late Quaternary glacial/interglacial  
1018 changes in sediment composition at the East Greenland continental margin and their  
1019 paleoceanographic implications. *Marine Geology* 122, 243-262.
- 1020 Norðdahl, H., Ingólfsson, O., 2015. Collapse of the Icelandic ice sheet controlled by  
1021 sealevel rise? *Arktos*, 1 pp 1-18.
- 1022 O'Cofaigh, C., Taylor, J., Dowdeswell, J.A., Rosell-Mele, A., Kenyon, N.H., Evans, J.,  
1023 Mienert, J., 2002. Geological evidence for sediment reworking on high-latitude  
1024 continental margins and its implications for palaeoceanography: insights from the  
1025 Norwegian– Greenland Sea. In: Dowdeswell, J.A., Ó Cofaigh, C. (Eds.),  
1026 *Glacierinfluenced sedimentation on high-latitude continental margins*. Geological Society  
1027 London Special Paper, 20. Geological Society, London, pp. 325–348.
- 1028 Paillard, D., Labeyrie, L., Yiou, P., 1996. Macintosh program performs time-series  
1029 analysis. *EOS* 77, 379.
- 1030 Patton, H., Hubbard, A., Bradwell, T., Schomacker, A., 2017. The configuration,  
1031 sensitivity and rapid retreat of the Late Weischelian Icelandic Ice Sheet.  
1032 *EarthScience Reviews* 166, 223-245.
- 1033 Petersen, S.V., Schrag, D.P., Clark, P.U., 2013. A new mechanism for  
1034 DansgaardOeschger cycles. *Paleoceanography* 28, 24-30.

- 1035 Phillips, R.L., Grantz, A., 2001. Regional variations in provenance and abundance of  
1036 icerafted clasts in Arctic Ocean sediments: implications for the configuration of late  
1037 Quaternary oceanic and atmospheric circulation in the Arctic. *Marine Geology* 172,  
1038 91-115.
- 1039 Pickart, R.S., Torres, D.J., Fratantoni, P.S., 2005. the East Greenland spill jet. *Journal of*  
1040 *Physical Oceanography* 35, 1037-1053.
- 1041 Prah, F.G., Muelhausen, L.A., Zahnle, D.L., 1988, Further evaluation of long-chain  
1042 alkenones as indicators of paleoceanographic conditions. *Geochimica et*  
1043 *Cosmochimica Acta* 52, 2303-2310.
- 1044 Rasmussen, S.O., Bigler, M., Blockley, S.P., Blunier, T., Buchardt, S.L., Clausen, H.B.,  
1045 Cvijanovic, I., Dahl-Jensen, D., Johnsen, S.J., Fischer, H., Gkinis, V., Guillevic, M.,  
1046 Hoek, W.Z., Lowe, J.J., Pedro, J.B., Popp, T., Seierstad, I.K., Steffensen, J.P.,  
1047 Svensson, A.M., Vallenga, P., Vinther, B.M., Walker, M.J.C., Wheatley, J.J.,  
1048 Winstrup, M., 2014. A stratigraphic framework for abrupt climatic changes during  
1049 the Last Glacial period based on three synchronized Greenland ice-core records:  
1050 refining and extending the INTIMATE event stratigraphy. *Quaternary Science*  
1051 *Reviews* 106, 14-28.
- 1052 Rasmussen, T.L., Wastegard, S., Kuijpers, A., van Weering, T.C.E., Heinemeier, J.,  
1053 Thomsen, E., 2003. Stratigraphy and distribution of tephra layers in marine sediment  
1054 cores from the Faeroe Islands, North Atlantic. *Marine Geology* 199, 263-277.
- 1055 Reeh, N., 2004. Holocene climate and fjord glaciations in Northeast Greenland:  
1056 implications for IRD deposition in the North Atlantic. *Sedimentary Geology* 165,  
1057 333-342.
- 1058 Reeh, N., Mayer, C., Miller, H., Thomsen, H.H., Weidick, A., 1999. Present and past  
1059 climate control on fjord glaciations in Greenland: Implications for IRD-deposition in  
1060 the sea. *Geophysical Research Letters* 26, 1039-1042.
- 1061 Reimer, P.J., Bard, E., Bayliss, A., Beck, J.W., Blackwell, P.G., Bronk Ramsey, C., Grootes,  
1062 P.M., Guilderson, T.P., Hafliadason, H., Hajdas, I., Hatt?, C., Heaton, T.J., Hoffmann, D.L.,  
1063 Hogg, A.G., Hughen, K.A., Kaiser, K.F., Kromer, B., Manning, S.W., Niu, M., Reimer,  
1064 R.W., Richards, D.A., Scott, E.M., Southon, J.R., Staff, R.A., Turney, C.S.M. and van

- 1065           der Plicht, J. (2013) IntCal13 and Marine13 Radiocarbon Age Calibration Curves 0-  
1066           50,000 Years cal BP. *Radiocarbon*, 55, 1869-1887.
- 1067   Robinson, S.G., Maslin, M.A., McCave, I.N., 1995. Magnetic susceptibility variations in  
1068           Upper Pleistocene deep-sea sediments of the N.E. Atlantic: Implications for ice  
1069           rafting and palaeocirculation at the Last Glacial Maximum. *Paleoceanography* 10,  
1070           221-250.
- 1071   Roesch, A. and Schmidbauer, H.W.C., 2018: WaveletComp: Computational Wavelet  
1072           Analysis. R package 1.1. <https://CRAN.R-project.org/package=Wavelet.Comp>.
- 1073   Ruddiman, W.F., McIntyre, A., 1981. The North Atlantic Ocean during the last  
1074           deglaciation. *Palaeogeography, Palaeoclimatology, Palaeoecology* 35, 145-214.
- 1075   Sadatzki, H., Maffezzoli, N., Dokken, T.M., Simon, M.H., Berben, S.M.P., Fahl, K.,  
1076           Kjær, H.A., Spolaor, A., Stein, R., Vallelonga, P., Vinther, P.M., Jansen, E., 2020.  
1077           Rapid reductions and millennial-scale variability in Nordic Seas sea ice cover during  
1078           abrupt glacial climate changes. *Proceedings of the National Academy of Sciences*  
1079           202005849. doi.org/10.1073/pnas.2005849117.
- 1080   Sarnthein, M., Winn, K., Jung, S., Duplessy, J. C., Labeyrie, L., Erlenkeuser, H., and  
1081           Ganssen, G., 1994. Changes in East Atlantic deepwater circulation over the last  
1082           30,000 years – An eight-time-slice record. *Paleoceanography* 9, 209–267.
- 1083   Sarnthein, M., Pflaumann, U., Weinelt, M., 2003. Past extent of sea ice in the northern  
1084           North Atlantic inferred from foraminiferal paleotemperature estimates.  
1085           *Paleoceanography* 18, doi:10.1029/2002PA000771.
- 1086   Schlitzer, R., 2011. Ocean Data View, <http://odv.awi.de,2011>.
- 1087
- 1088   Sejrup, H.P., Sioholm, J., Furnes, H., Beyer, I., Eide, L., Jansen, E., Mangerud, J., 1989.  
1089           Quaternary tephrochronology on the Iceland Plateau, north of Iceland. *Journal of*  
1090           *Quaternary Science* 4, 109-114.
- 1091   Shaffer, G., S.M. Olsen, and C.J. Bjerrum, 2004. Ocean subsurface warming as a  
1092           mechanism for coupling Dansgaard-Oeschger climate cycles and ice-rafting events.  
1093           *Geophysical Research Letters* 31, L24202, doi:10.1029/2004GL020968.

- 1094 Sicre, M.-A., Bard, E., Ezat, U., Rostek, F., 2002. Alkenone distributions in the North  
1095 Atlantic and Nordic sea surface waters. *Geochemistry, Geophysics, Geosystems*,  
1096 Article 2001GC000159.
- 1097 Sicre, M.-A., Labeyrie, L., Ezat, U., Duprat, J., Turon, J.-L., Schmidt, S., Michel, E.,  
1098 Mazaud A., 2005. Southern Indian Ocean response to Northern Hemisphere Heinrich  
1099 events. *Earth and Planetary Science Letters* 240, 724-731, doi: 10.1016.
- 1100 Sicre, M.-A., Jacob, J., Ezat, U., Rouse, S., Kissel, C., Yiou, P., Eiriksson, J., Knudsen,  
1101 K.-L., Jansen, E., Turon, J.-L., 2008a. Decadal variability of sea surface temperatures  
1102 off North Iceland over the last 2000 years. *Earth and Planetary Science Letters* 268,  
1103 137-142.
- 1104 Sicre, M.-A., Yiou, P., Eiriksson, J., Ezat, U., Guimbaut, E., Dahhaoui, I., Knudsen, K.L.,  
1105 Jansen, E., Turon, J.-L., 2008b. A 4500-year reconstruction of sea surface  
1106 temperature variability at decadal time scales off North Iceland. *Quaternary Science*  
1107 *Reviews* 27, 2041-2047.
- 1108 Simon, Q., Hillaire-Marcel, C., St-Onge, G., Andrews, J.T., 2014. North-eastern  
1109 Laurentide, western Greenland and southern Inuitian ice stream dynamics during  
1110 the last glacial cycle. *Journal of Quaternary Science* 29, 14-26.
- 1111 Skinner L.C. & I.N. McCave. Analysis and modelling of the behaviour of gravity and  
1112 piston corers based on soil mechanical principles. *Marine Geology* 199, 181-204.
- 1113 Skinner, L. C., Muschitiello, F., & Scrivner, A. E., 2019. Marine reservoir age variability  
1114 over the last deglaciation: Implications for marine carbon cycling and prospects for  
1115 regional radiocarbon calibrations. *Paleoceanography and Paleoclimatology* 34,  
1116 1807–1815. <https://doi.org/10.1029/2019PA003667>
- 1117 Stefansson, U., 1962. North Icelandic Waters. *Rit Fiskideildar III. Bind, Vol 3*, 269.
- 1118 Stein, R., 2008. *Arctic Ocean Sediments. Processes, Proxies, and Paleoenvironment*.  
1119 Elsevier, New York.
- 1120 Stein, R., Nam, S.-I., Grobe, H., Hubberten, H., 1996a. Late Quaternary glacial history  
1121 and short-term ice-rafted debris fluctuations along the East Greenland continental  
1122 margin, in: Andrews, J.T., Austin, W.A., Bergsten, H., Jennings, A.E. (Eds.), *Late*

- 1123 Quaternary paleoceanography of North Atlantic margins. Geological Society,  
1124 London, pp. 135-151.
- 1125 Stein, R., Nam, S.-Il., Grobe, H., Hubberten, Hans-Wolfgang, H., 1996b. Sedimentology  
1126 and stable isotope ratios of cores from the East Greenland continental margin.  
1127 *PANGAEA*, <https://doi.org/10.1594/PANGAEA.733965>,
- 1128 Stokes, C.R., Clark, C.D., Darby, D.A., Hodgson, D.A., 2005. Late Pleistocene ice export  
1129 events into the Arctic Ocean from the M'Clure Strait Ice Stream, Canadian Arctic  
1130 Archipelago. *Global and Planetary Change* 49, 139-162.
- 1131 Telford, R.J., Heegaard, E., Birks, H.J.B., 2003. All age-depth models are wrong: but  
1132 how badly? *Quaternary Science Reviews* 23, 1-5.
- 1133 Trachsel, M., Telford, R.J., 2017 All age-depth models are wrong, but are getting better.  
1134 *Holocene* 27, 860-869 van Kreveld, S., Sarthein, M., Erlenkeuser, H.,  
1135 Grootes, P., Jung, S., Nadeau, M.J.,  
1136 Pflaumann, U., Voelker, A., 2000. Potential links between surging ice sheets,  
1137 circulation changes, and the Dansgaard-Oeschger cycles in the Irminger Sea, 60-18  
1138 ka. *Paleoceanography* 15, 425-442.
- 1139 Vasskog, K., Langebroek, P.M., Andrews, J.T., Nilsen, J.E.O., Nesje, A., 2015. The  
1140 Greenland Ice Sheet during the last glacial cycle: Current ice loss and contribution to  
1141 sea-level rise from a palaeoclimatic perspective. *Earth-Science Reviews* 150, 45-67.
- 1142 Velay-Vitow, J., Peltier, W.R., and Stuhne, G. , 2019. Tides of the Glacial Ocean and  
1143 their role in Heinrich Event instability. *Geophysical Research Abstracts*. 21,  
1144 EGU2019-3733.
- 1145 Venkatesh, S., Murphy, D.L., Wright, G.F., 1994. On the deterioration of icebergs in the  
1146 marginal ice-zone. *Atmosphere-Ocean* 32, 469-484.
- 1147 Verplanck, E.P., Farmer, G.L., Andrews, J., Dunhill, G., Millo, C., 2009. Provenance of  
1148 Quaternary glacial and glacial marine sediments along the southeast Greenland margin.  
1149 *Earth and Planetary Science Letters* 286, 52-62.
- 1150 Voelker, A.H.L., 1999. Zur Deutung der Dansgaard-Oeschger Ereignisse in  
1151 ultrahochauflösenden Sedimentprofilen aus dem Europäischen Nordmeer,  
1152 Dansgaard-Oeschger events in ultra-high resolution sediment records from the Nordic  
1153 Seas.

- 1154           Universitat Kiel, Kiel, p. 271.
- 1155   Voelker, A.H.L., Grootes, P.M., Nadeau, M-J., and Sarnthein, M., 2000. Radiocarbon  
1156           levels in the Iceland Sea from 25–53 kyr and their link to the earth’s magnetic field  
1157           intensity. Radiocarbon 42, p 437–452
- 1158   Voelker, A.H.L., Haflidason, H., 2015. Refining the Icelandic tephrochronology of the  
1159           last glacial period - The deep-sea core P52644 record from the southern Greenland  
1160           Sea. Global and Planetary Change 131, 35-62.
- 1161   Voelker, A.H.L., Sarnthein, M., Grootes, P.M., Erlenkeuser, H., Laj, C., Mazaud, A.,  
1162           Nadeau, M-J., Schleicher, M., 1998: Correlation of marine <sup>14</sup>C ages from the Nordic  
1163           Seas with the GISP2 isotope record: implications for <sup>14</sup>C calibration beyond 25 ka  
1164           BP. Radiocarbon 40, 517-534.
- 1165   Volkman, J.K., 1986. A review of sterol markers for marine and terrigenous organic  
1166           matter. Organic Geochemistry 9, 83–99.
- 1167   Vogt, C., 2017. Bulk mineral assemblage via Quantitative Phase Analysis with X-ray  
1168           diffraction of sediment core PS2644-5 KAL. PANGAEA.  
1169           <https://doi.org/10.1594/PANGAEA.875919>
- 1170   Walczuk, M.H. & 13 others, 2020. Phasing of millennial-scale climate variability in the  
1171           Pacific and Atlantic oceans. Science, 370, 716–720.
- 1172   Watkins, S.J., Maher, B.A., 2003. Magnetic characterization of present-day deep-sea  
1173           sediments and sources in the North Atlantic. Earth and Planetary Science Letters 214,  
1174           379-394.
- 1175   White, L.F., Bailey, I., Foster, G.L., Allen, G., Kelley, S.P., Andrews, J.T., Hogan, K.,  
1176           Dowdeswell, J.A., Storey, C.D., 2016. Tracking the provenance of  
1177           Greenland-sourced, Holocene aged, individual sand-sized ice-rafted debris using the  
1178           Pb-isotope compositions of feldspars and Ar-40/Ar-39 ages of hornblendes. Earth  
1179           and Planetary Science Letters 433, 192-203.
- 1180   Xiao, X., Fahl, K., Stein, R., 2013. Biomarker distributions in surface sediments from the  
1181           Kara and Laptev seas (Arctic Ocean): indicators for organic-carbon sources and  
1182           seaice coverage. Quaternary Science Reviews 79, 40–52.

1183 Xiao, X., Zhao, M., Knudsen, K.L., Sha, L., Eiríksson, J., Gudmundsdóttir, E., Jiang, H.,  
1184 Guo, Z., 2017. Deglacial and Holocene sea–ice variability north of Iceland and  
1185 response to ocean circulation changes. *Earth and Planetary Science Letters* 472, 14–  
1186 24.

1187 Zou, H., 2016. An X-Ray Diffraction Approach: Bulk Mineral Assemblages as  
1188 Provenance Indicator of Sediments from the Arctic Ocean. University of Bremen,  
1189 Bremen, pp. 116. <https://elib.suub.uni-bremen.de/edocs/00105354-1.pdf>.

1190  
1191

1192  
1193

## Methods

1194

1195 **Magnetic susceptibility:** Magnetic susceptibility was measured on-board the *Marion*  
1196 *Dufresne* (Labeyrie and Cort, 2005) in 2-cm increments (hence ~150yr sampling on  
1197 average). Measurements were taken on the 1.5 m core sections. In this area of Iceland, the  
1198 marine deposits are strongly affected by erosion and transport of basalt, which results in  
1199 very high values of magnetic susceptibility. The export of sediments from the erosion of  
1200 bedrock with much lower magnetic susceptibilities, such as granites and other felsicrich  
1201 bedrock in NE Greenland and from more distant sources (Verplanck et al., 2009; White et  
1202 al., 2016) will lower the magnetic susceptibility readings. It is important to note that  
1203 although magnetic susceptibility is straightforward to measure, data interpretation is  
1204 complex, being a product of sediment density, grain-size, and mineralogy (Robinson et  
1205 al., 1995; Stoner and Andrews, 1999; Watkins and Maher, 2003).

1206 **Quantitative X-ray Diffraction (qXRD):** The weight % (wt%) of the non-clay  
1207 and clay mineral composition of the < 2 mm sediment fractions is based on the US



1208 Geological Survey method (Eberl, 2003), which has been used extensively in this region  
1209 (e.g. Andrews et al., 2017; Andrews and Eberl, 2007; Andrews and Vogt, 2014). One  
1210 gram of sediment (dry weight) is spiked with 0.111 g of zincite, prepared (Eberl, 2003),  
1211 run in the X-ray diffractometer, and the resulting intensity data processed in the Excel  
1212 macro-program Rockjock v6. We investigate the wt% and presence/absence of 34  
1213 minerals and reduced this number by combining individual mineral wt% into larger  
1214 groups, such as k-feldspars, plagioclase, dolomite, and amorphous minerals. Importantly  
1215 in the context of this paper we had earlier shown that qXRD can recognize the presence  
1216 of tephra and volcanic glass, with some ability to distinguish between basaltic and  
1217 rhyolitic glass (Andrews et al., 2013).

1218         To gain a better understanding of possible changes in the provenance of the  
1219 mineral compositions we processed the mineral wt% data in a sediment unmixing  
1220 program “SedUnMix” (Andrews and Eberl, 2012). Two models were considered, the first  
1221 with qXRD results from #2274 with four appropriate bedrocks, namely: basalt, dolerite,  
1222 gneiss, and granite; and secondly with the mineral compositions of glacial marine  
1223 sediment samples from potential source areas, namely: NE Greenland, E. Greenland, and  
1224 Iceland (Suppl. Table of bedrock and marine sediment sources). The program calculates a  
1225 “degree of fit” and also derives error estimates on each source within a sample. Ideally,  
1226 the sum of the sources should equal 100% but marked deviations from this suggest that  
1227 one or more sources have not been included, and/or that the sources are not representative  
1228 of the sediment samples.

1229         **Grain-size:** Sediment was wet-sieved at 2 mm and the grain-size volume  
1230 percentages in 96 intervals between 0.01 and 2000  $\mu\text{m}$  were obtained via a Malvern laser

1231 system. Comparisons between the Malvern and other grain-size systems have been  
1232 documented and found comparable (McCave et al., 2006; McCave and Syvitski, 1991).  
1233 However, the objections of McCave et al. (2006) to laser sizers on the grounds of grain  
1234 shape (Konert and Vandenberghe, 1997) are not valid for equant grains such as those  
1235 produced by glacial grinding, as pointed out by Piper (Marshall et al., 2014), and thus  
1236 size data are believed valid in the setting of MD2274. Grain-size curves have provided  
1237 vital information on sediment transport and deposition in this region, and methods have  
1238 been developed to reconstruct variations in bottom current speed for sediments delivered  
1239 to the ocean from dominantly glacial sources (McCave and Andrews, 2019a, b) The  
1240 calibration of sortable silt mean (mean of 10-63  $\mu\text{m}$ ), a sensitivity, by McCave et  
1241 al.,(2017) has been applied to changes in the grainsize record.

1242 **Biomarkers:** Biomarkers were extracted from freeze-dried subsamples (~2-4 g).  
1243 Prior to extraction, samples were spiked with an internal standard (9-octylheptadec-8-ene,  
1244 9-OHD, 10  $\mu\text{L}$ ; 10  $\mu\text{g mL}^{-1}$ ) to permit quantification of the highly branched isoprenoid  
1245 (HBI) biomarkers IP<sub>25</sub>, HBI II and HBI III. 5 $\alpha$ -androstan-3 $\beta$ -ol; (0.1  $\mu\text{g}$ ) was also added  
1246 to permit quantification of brassicasterol in some cases. Samples were then saponified in  
1247 a methanolic KOH solution (~5 mL H<sub>2</sub>O:MeOH (1:9); 5% KOH) for 60 min (70 °C).  
1248 Hexane (3 $\times$ 2 mL) was added to the saponified mixtures, with supernatant solutions,  
1249 containing non-saponifiable lipids (NSLs), transferred by glass pipettes to glass vials, and  
1250 solvent removed using a gentle stream of N<sub>2</sub>. Dried NSLs were re-suspended in hexane  
1251 (0.5 mL) and fractionated using column chromatography (SiO<sub>2</sub>; 0.5 g). Non-polar lipids,  
1252 including IP<sub>25</sub> and HBI II, were eluted with hexane (6 mL), while more polar lipid  
1253 fractions containing alkenones were eluted with MeOH (6 mL). For a few horizons,

1254 additional NSLs were fractionated to yield non-polar (hexane; 6 mL) and polar fractions  
1255 containing sterols (hexane:methyl acetate 4:1; 6 mL). Each non-polar fraction was further  
1256 purified to remove saturated components using silver-ion chromatography (Belt et al.,  
1257 2015), with saturated compounds eluted with hexane (2 mL) and unsaturated compounds,  
1258 including IP<sub>25</sub> and other HBIs, collected in a subsequent acetone fraction (3 mL).  
1259 Analysis of fractions containing IP<sub>25</sub> and other HBIs was carried out using gas  
1260 chromatography–mass spectrometry (GC–MS) following the methods and operating  
1261 conditions described previously (Belt et al., 2012). Mass spectrometric analysis was  
1262 carried out in total ion current (TIC) and selected ion monitoring (SIM) modes. The  
1263 identification of IP<sub>25</sub> and HBI II was based on their characteristic GC retention indices  
1264 (e.g. RI<sub>HP5MS</sub> = 2081,2082 and 2044 for IP<sub>25</sub>, HBI II and HBI III, respectively) and mass  
1265 spectra (Belt, 2018). Quantification of all HBIs was achieved by comparison of mass  
1266 spectral responses of selected ions (e.g. IP<sub>25</sub>, *m/z* 350; HBI II, *m/z* 348; HBI III, *m/z* 346)  
1267 in SIM mode with those of the internal standard (9-OHD, *m/z* 350) and normalized  
1268 according to their respective instrumental response factors, derived from solutions of  
1269 known biomarker concentration, and sediment masses (Belt et al., 2012). Fractions  
1270 containing sterols were derivatized with N,O-bis(trimethylsilyl)trifluoroacetamide  
1271 (BSTFA; 100 µL; 70°C for 60 min) immediately prior to analysis by GC–MS. Sterols  
1272 were identified by comparison with GC–MS responses compared to those of standards.  
1273 Sterol quantification was achieved as per the approach described above for HBIs.

1274 Polar fractions containing alkenones obtained from elution with MeOH (6 mL) were  
1275 further purified with 2 mL of hexane:methyl acetate (95:5 v/v) and 2 mL of hexane:methyl  
1276 acetate (90:10 v/v). Alkenones were analyzed using a Thermo Trace GC Ultra gas

1277 chromatograph equipped with a CPSil5 capillary column (50m length, 0.32 i.d. and 0.25  
1278 mm film thickness), an FID detector and a septum programmable injector (SPI). Helium  
1279 was used as carrier gas. 5 $\alpha$ -cholestane was added as an external standard prior to GC  
1280 injection. SST estimates were determined using the following equation (Prah1 et al., 1988).

1281  
1282

$$1283 \quad K' \quad C_{\text{chole}} \\ 1284 \quad U37 \quad \frac{C_{\text{chole}}}{C_{\text{chole}} + C_{\text{ster}}} = 0.034 T + 0.039 \\ 1285$$

1286

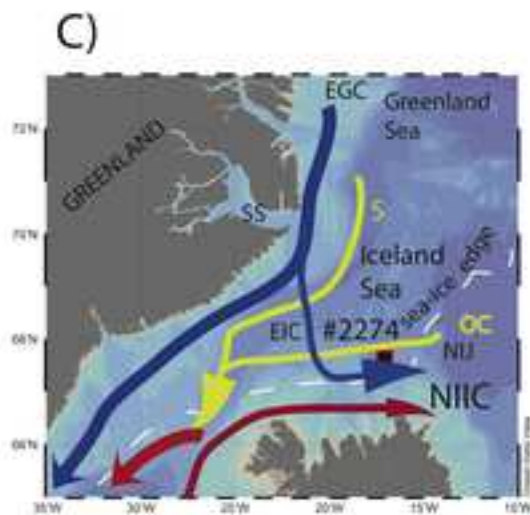
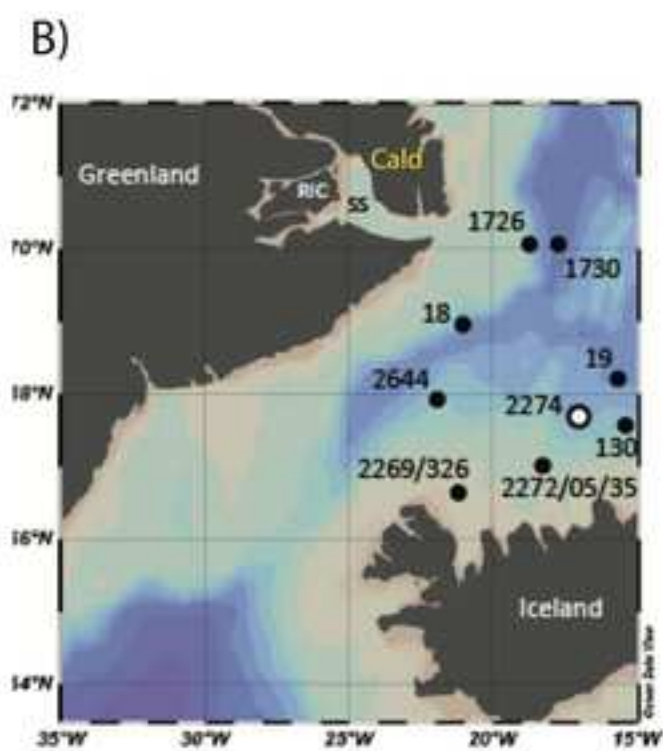
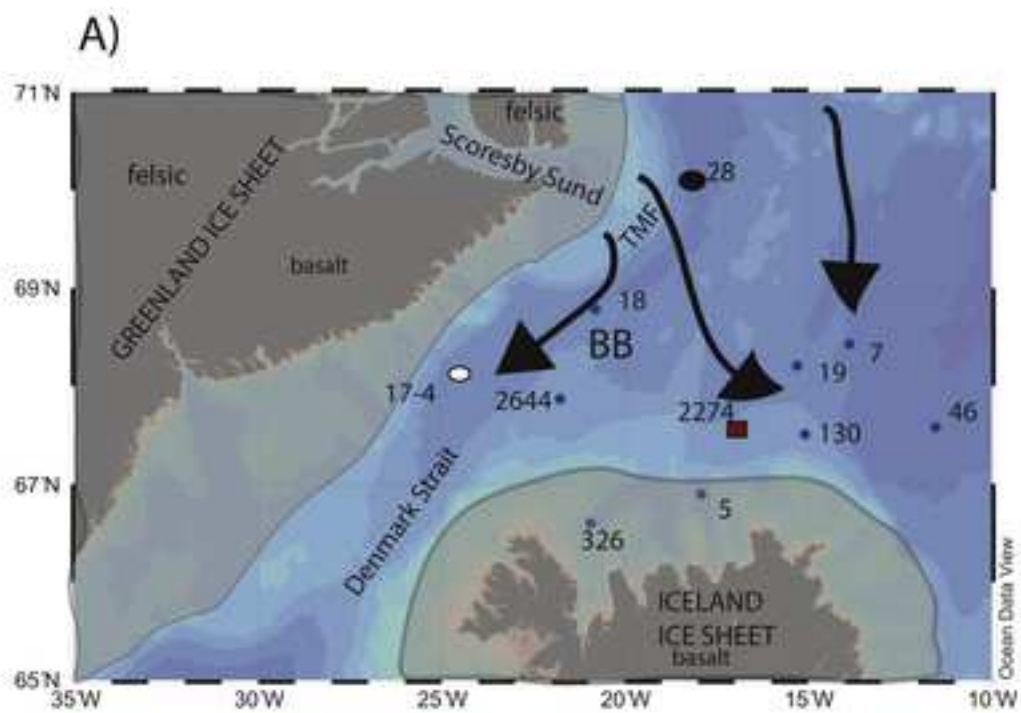
## 1287 **References**

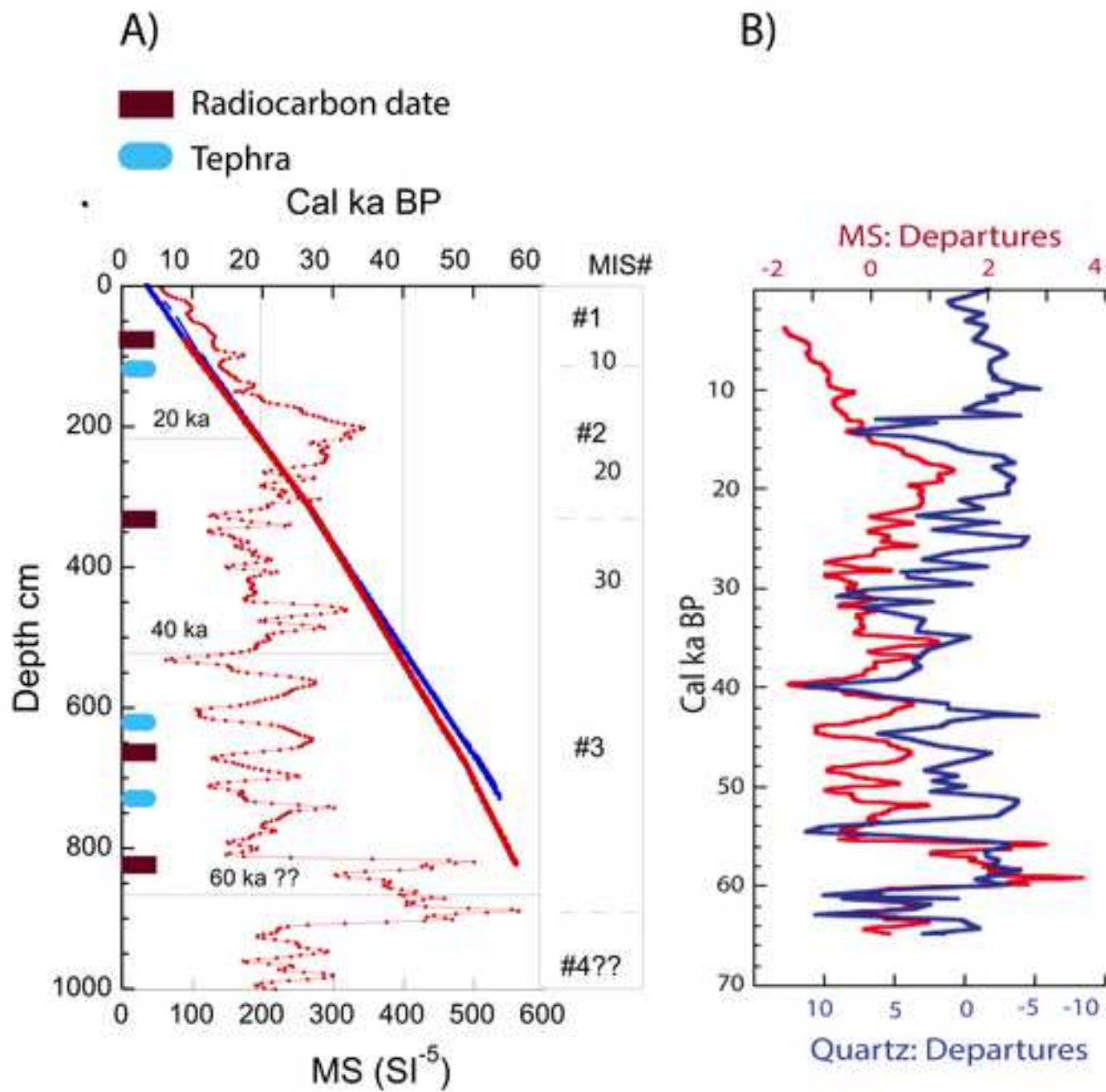
- 1288 Andrews, J.T., Dunhill, G., Vogt, C., Voelker, A.H.L., 2017. Denmark Strait during the  
1289 Late Glacial Maximum and Marine Isotope Stage 3: Sediment sources and transport  
1290 processes. *Marine Geology* 390, 181-198.
- 1291 Andrews, J.T., Eberl, D.D., 2007. Quantitative mineralogy of surface sediments on the  
1292 Iceland shelf, and application to down-core studies of Holocene ice-rafted sediments.  
1293 *Journal of Sedimentary Research* 77, 469-479.
- 1294 Andrews, J.T., Eberl, D.D., 2012. Determination of sediment provenance by unmixing  
1295 the mineralogy of source-area sediments: The "SedUnMix" program. *Marine*  
1296 *Geology* 291, 24-33.
- 1297 Andrews, J.T., Vogt, C., 2020. Variations in felsic- versus mafic-sources in the Western  
1298 Nordic Seas during MIS 1 to MIS 4 *Marine Geology* 424, 106164.
- 1299 Belt, S.T., 2018. Source-specific biomarkers as proxies for Arctic and Antarctic sea ice,  
1300 *Organic Geochemistry* 125, 277–298, doi: 10.1016/j.orggeochem.2018.10.002.
- 1301 Belt, S.T., Brown, T.A., Navarro-Rodriguez, A., Cabedo-Sanz, P., Tonkin, A., Ingle, R.,  
1302 2012. A reproducible method for the extraction, identification and quantification of  
1303 the Arctic sea ice proxy IP<sub>25</sub> from marine sediments. *Analytical Methods* 4, 705–713.

- 1304 Belt, S.T., Cabedo-Sanz, P., Smik, L., Navarro-Rodriguez, A., Berben, S.M. P., Knies, J.,  
1305 Husum, K., 2015. Identification of paleo Arctic winter sea ice limits and the marginal  
1306 ice zone: optimised biomarker-based reconstructions of late Quaternary Arctic sea  
1307 ice. *Earth and Planetary Science Letters* 431, 127-139.
- 1308 Eberl, D.D., 2003. User guide to RockJock: A program for determining quantitative  
1309 mineralogy from X-ray diffraction data. United States Geological Survey, Open File  
1310 Report 03-78, 40 pp, Washington, DC.
- 1311 Konert, M., Vandenberghe, J., 1997. Comparison of laser grain size analysis with pipette  
1312 and sieve analysis: a solution for the underestimation of the clay fraction.  
1313 *Sedimentology* 44, 523-535.
- 1314 Marshall, N.R., Piper, D.J.W., Saint-Ange, F., Campbell, D.C., 2014. Late Quaternary  
1315 history of contourite drifts and variations in Labrador Current flow, Flemish Pass,  
1316 offshore eastern Canada. *Geology Marine Letters* 34, 457-470.  
1317 doi:10.1007/s00367014-0377-z.
- 1318 McCave, I.N., Andrews, J.T., 2019a. Distinguishing current effects in sediments  
1319 delivered to the ocean by ice. I. Principles, methods and examples. *Quaternary*  
1320 *Science Reviews* 212, 92-107.
- 1321 McCave, I.N., Andrews, J.T., 2019b. Distinguishing current effects in sediments  
1322 delivered to the ocean by ice. II. Glacial to Holocene changes in North Atlantic high  
1323 latitude upper ocean flows. *Quaternary Science Reviews* 223, no. 105902, 21pp.
- 1324 McCave, I.N., Hall, I.R., Bianchi, G.G., 2006. Laser vs settling velocity differences in silt  
1325 grainsize measurements: estimation of palaeocurrent vigour. *Sedimentology* 53,  
1326 919-928.
- 1327 McCave, I.N., Manighetti, B. and Robinson, S.G., 1995. Sortable silt and fine sediment  
1328 size/composition slicing: parameters for palaeocurrent speed and palaeoceanography.  
1329 *Paleoceanography* 10, 593-610.
- 1330 McCave, I.N., Thornalley, D.J.R., Hall, I.R., 2017. Relation of sortable silt grain-size to  
1331 deep-sea current speeds: Calibration of the 'Mud Current Meter'. *Deep-Sea Research*  
1332 *Part I* 127, 1-12.

- 1333 McCave, I.N., Syvitski, J.P.M, 1991. Principles and methods of geological particle size  
1334 analysis, in: Syvitski, J.P.M. (Ed.), Principles, methods and application of particle  
1335 size analysis. Cambridge University Press, pp. 3-21.  
1336  
1337  
1338
- 1339 Robinson, S.G., Maslin, M.A., McCave, I.N., 1995. Magnetic susceptibility variations in  
1340 Upper Pleistocene deep-sea sediments of the N.E. Atlantic: Implications for ice  
1341 rafting and palaeocirculation at the Last Glacial Maximum. *Paleoceanography* 10,  
1342 221-250.
- 1343 Stoner, J.S., Andrews, J.T., 1999. The North Atlantic as a Quaternary magnetic archive,  
1344 in: Maher, B., Thompson, R. (Eds.), *Quaternary Climates, Environments and*  
1345 *Magnetism*. Cambridge University Press, Cambridge, UK, pp. 49-80.
- 1346 Verplanck, E.P., Farmer, G.L., Andrews, J., Dunhill, G., Millo, C., 2009. Provenance of  
1347 Quaternary glacial and glacial marine sediments along the southeast Greenland margin.  
1348 *Earth and Planetary Science Letters* 286, 52-62.
- 1349 Watkins, S.J., Maher, B.A., 2003. Magnetic characterization of present-day deep-sea  
1350 sediments and sources in the North Atlantic. *Earth and Planetary Science Letters* 214,  
1351 379-394.
- 1352 White, L.F., Bailey, I., Foster, G.L., Allen, G., Kelley, S.P., Andrews, J.T., Hogan, K.,  
1353 Dowdeswell, J.A., Storey, C.D., 2016. Tracking the provenance of  
1354 Greenland-sourced, Holocene aged, individual sand-sized ice-rafted debris using the  
1355 Pb-isotope compositions of feldspars and Ar-40/Ar-39 ages of hornblendes. *Earth*  
1356 *and Planetary Science Letters* 433, 192-203.  
1357  
1358

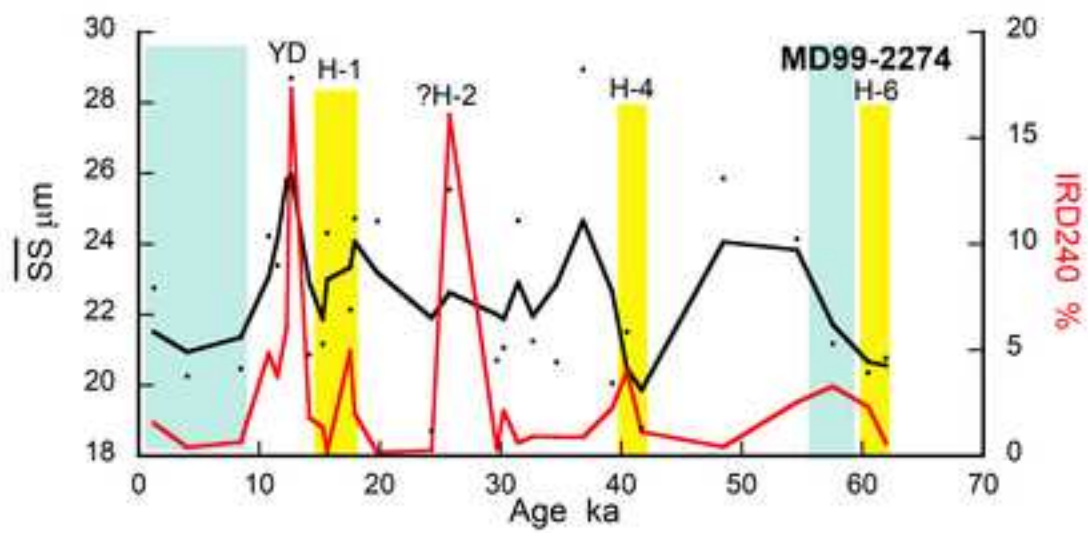
"Disclaimer: This is a pre-publication version. Readers are recommended to consult the full published version for accuracy and citation."



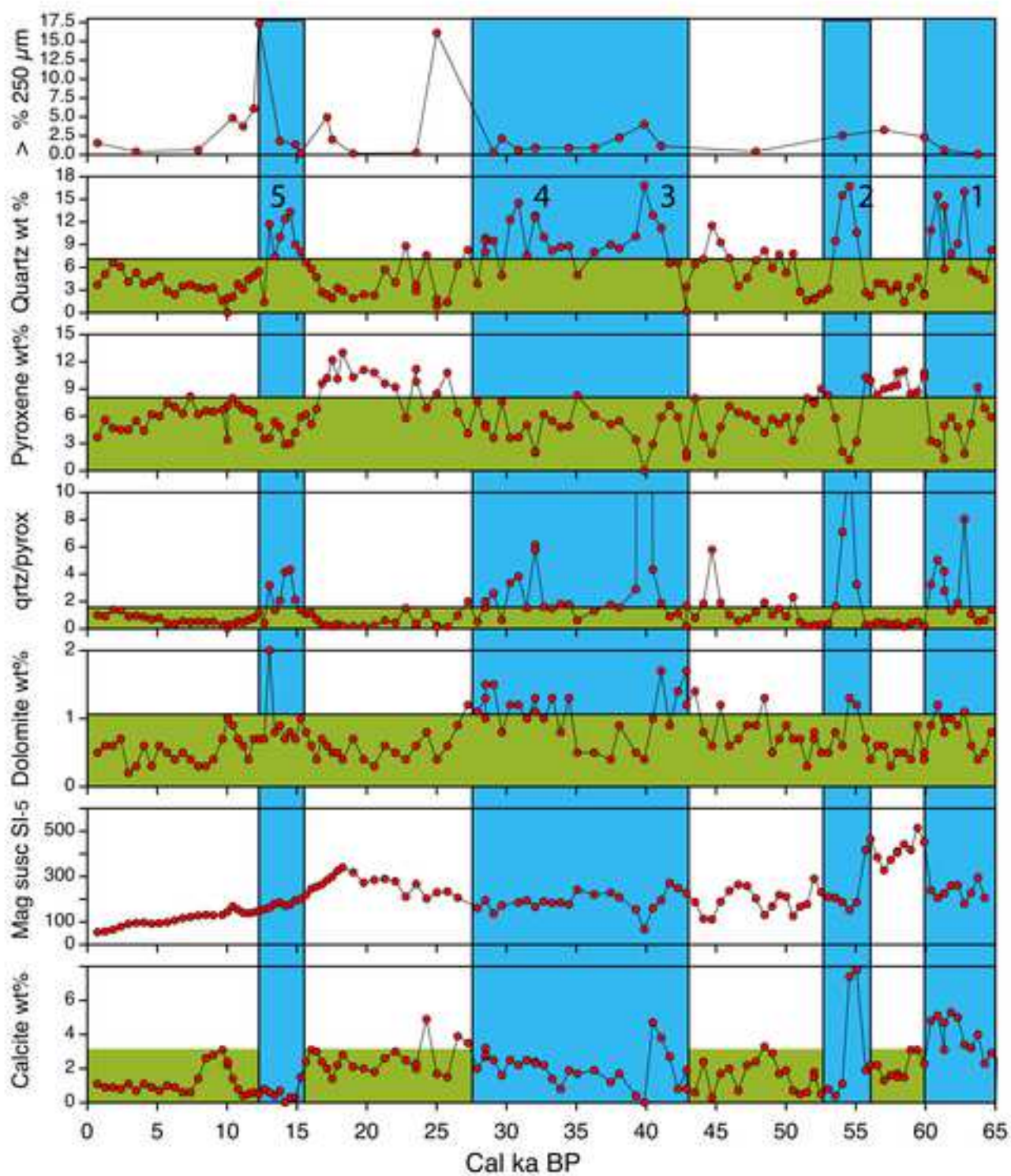




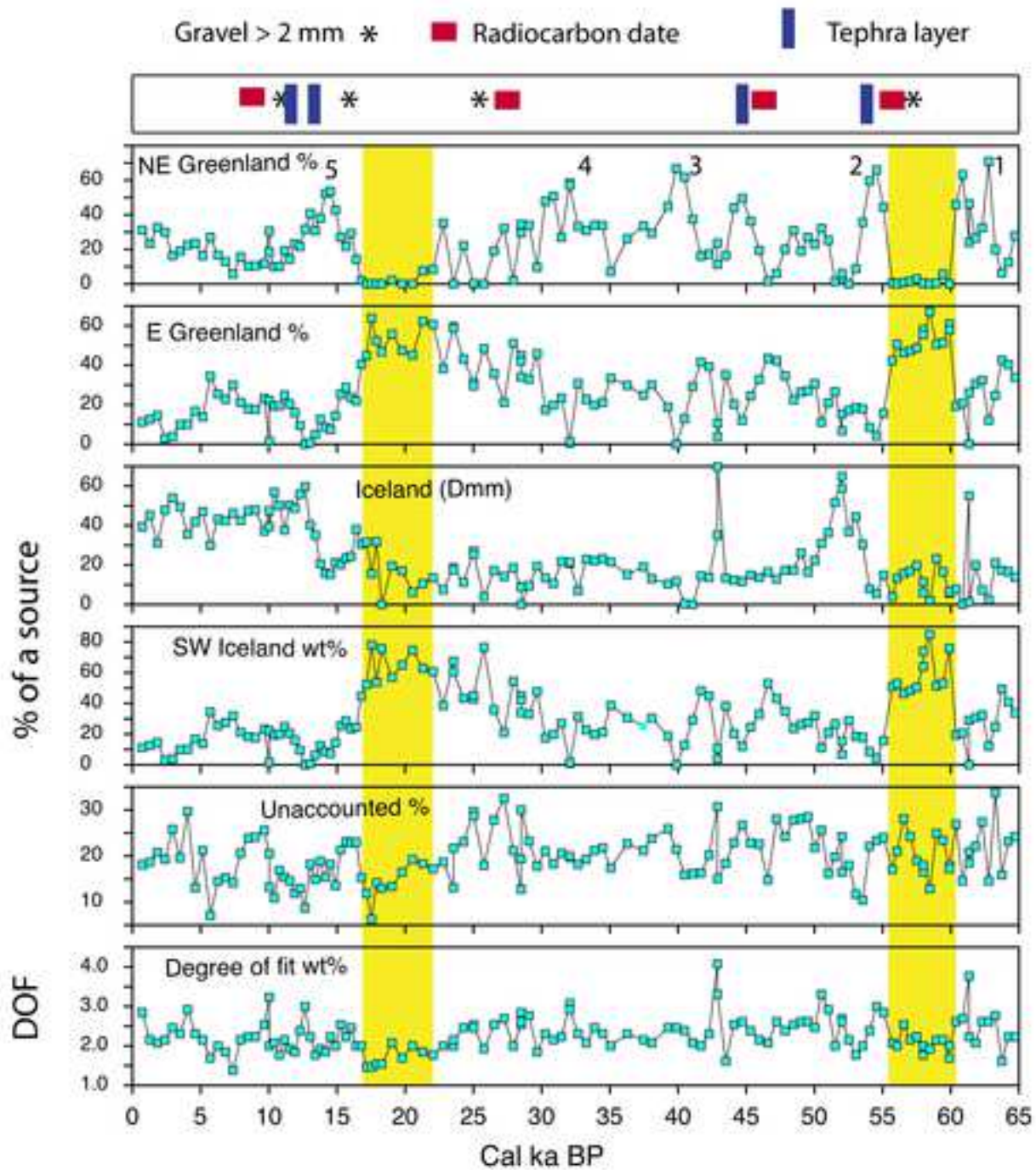
“Disclaimer: This is a pre-publication version. Readers are recommended to consult the full published version for accuracy and citation.”



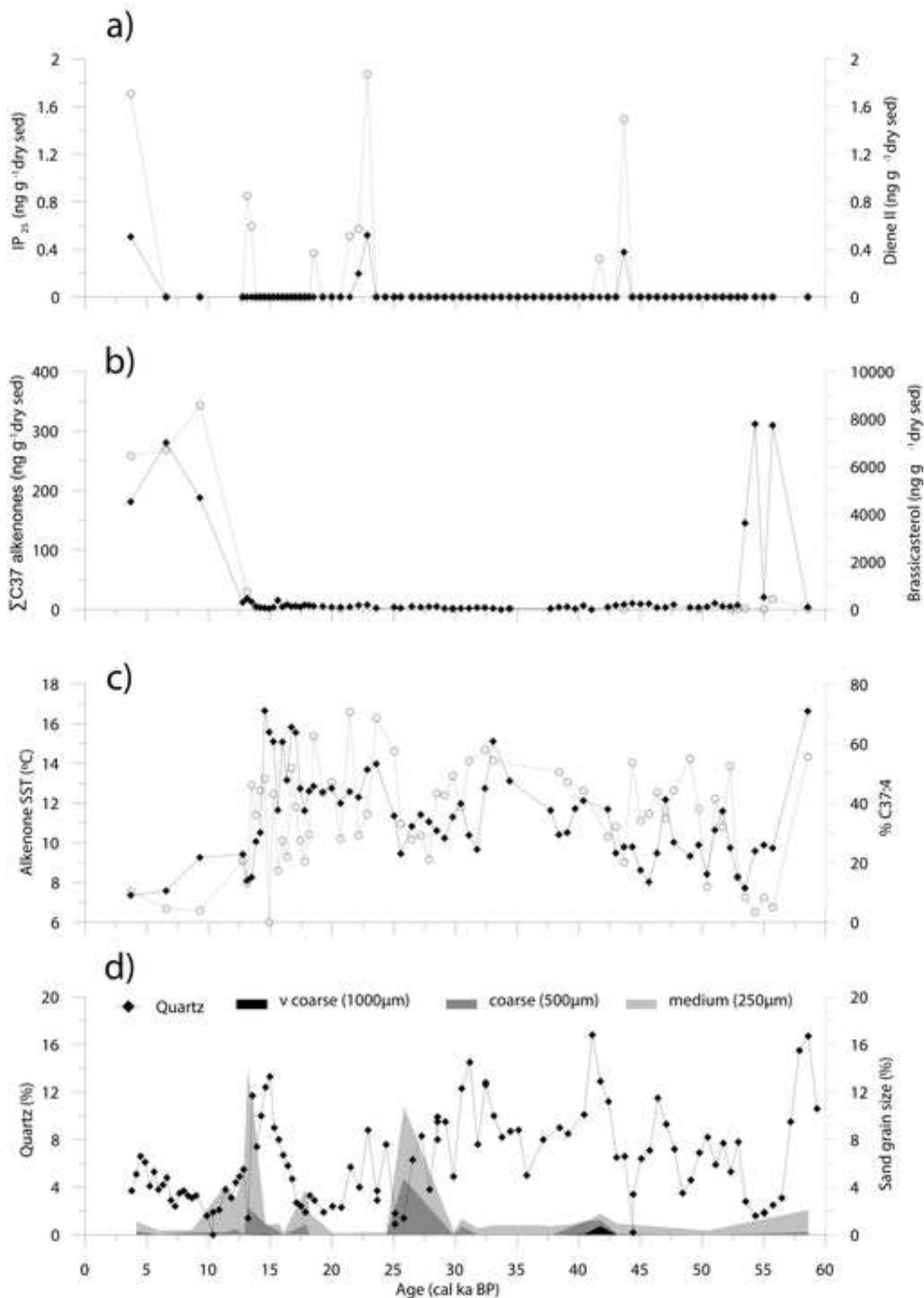
"Disclaimer: This is a pre-publication version. Readers are recommended to consult the full published version for accuracy and citation."



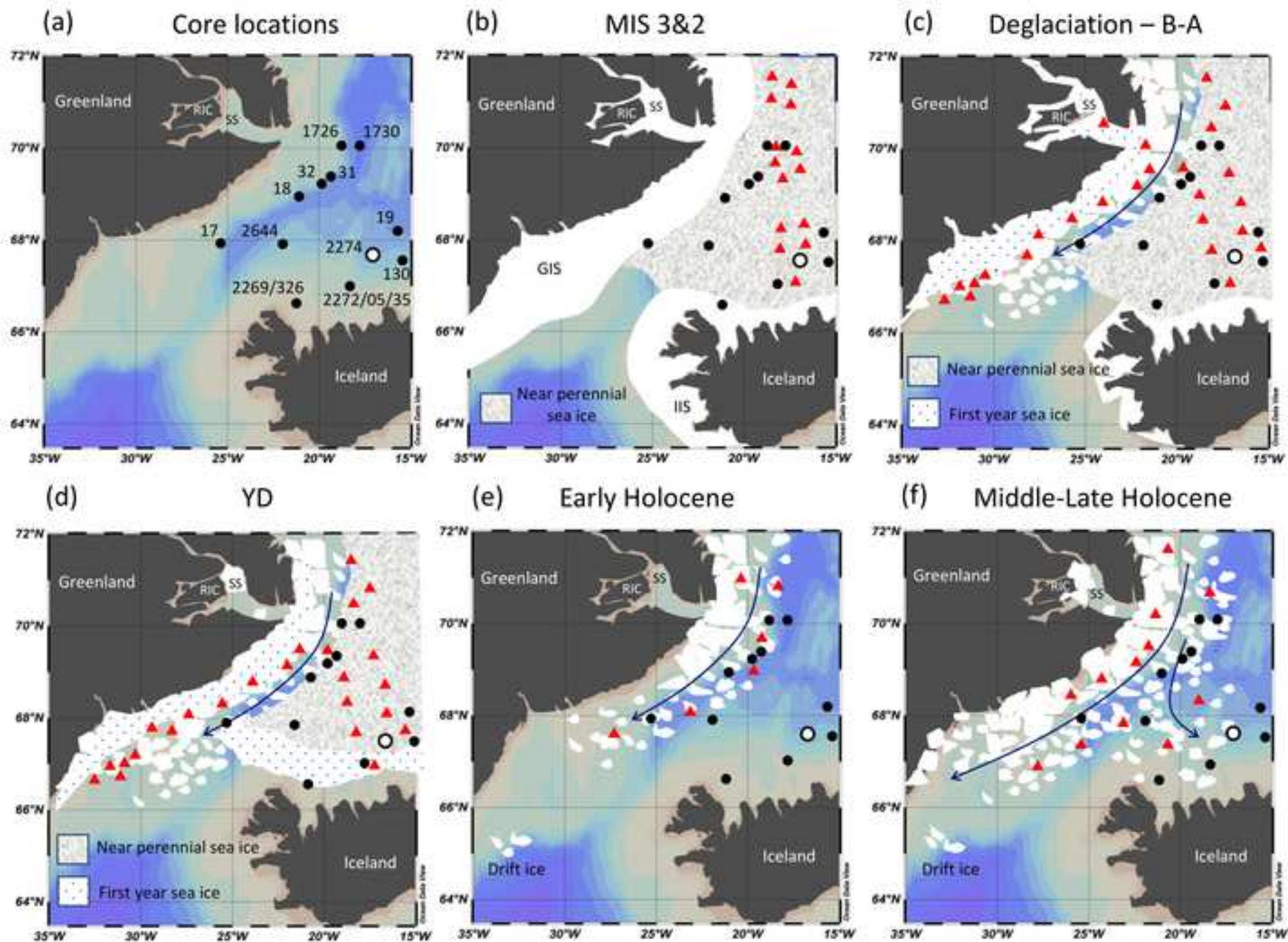
"Disclaimer: This is a pre-publication version. Readers are recommended to consult the full published version for accuracy and citation."



"Disclaimer: This is a pre-publication version. Readers are recommended to consult the full published version for accuracy and citation."



"Disclaimer: This is a pre-publication version. Readers are recommended to consult the full published version for accuracy and citation."



“Disclaimer: This is a pre-publication version. Readers are recommended to consult the full published version for accuracy and citation.”

